**Title**
High-Speed Dielectrophoresis and 3D Microfluidics for Biological Applications



**Author**
Kung, Yu-Chun

**Publication Date**
2016

Peer reviewed|Thesis/dissertation

UNIVERSITY OF CALIFORNIA

Los Angeles

# High-Speed Dielectrophoresis and 3D Microfluidics for Biological Applications

A dissertation submitted in partial satisfaction of the requirement for the degree of Doctor of Philosophy in Mechanical Engineering

by

Yu-Chun Kung

2016

ABSTRACT OF THE DISSERTATION

# High-Speed Dielectrophoresis and 3D Microfluidics for Biological Applications

by

Yu-Chun Kung

Doctor of Philosophy in Mechanical Engineering

University of California, Los Angeles, 2016

Professor Pei-Yu Chiou, Chair

The ability to manipulate biological cells and micrometer-scale particles plays an important role in many biological and colloidal science applications. However, conventional manipulation techniques, such as optical forces, electrokinetic forces (electrophoresis, dielectrophoresis (DEP), and traveling-wave dielectrophoresis), magnetic forces, acoustic forces (surface standing acoustic waves (SAW), and bulk standing acoustic waves(BAW)), and hydrodynamic flows, cannot achieve high resolution and high throughput at the same

time. While electrokinetic forces and other mechanisms provide higher throughput than optical mechanism, but lack the flexibility or the spatial resolution necessary for controlling individual particles. None of which could provide high resolution, throughput and versatility in clinical applications.

In this dissertation, I present a novel DEP concept for high resolution, throughput and versatility microns-sized particle and biological cell manipulation in high-speed flows. Using novel three-dimensional (3D) polydimethylsiloxane (PDMS) thin-film fabrication platform I developed, true heterogeneous integration of electronics on hard substrates (silicon and/or glass) and PDMS are demonstrated for the first time to create 3D electric field across the entire large area (couple centimeter across) 3D microfluidic channel networks. Which enables broad applications, such as sheathless sub-micron particle focusing in high-speed flows, tunable micron-sized particle and cell focusing in high-speed flows, and ultra-high precision particle size-

based sorting. Within all sections, experiments were performed with beads to verify the concept of each platform and then with cells to demonstrate qualitative and quantitative operation of the performance. These technologies is now well poised to enable the development of biological assays that are currently unavailable.

The dissertation of Yu-Chun Kung is approved.

Chih-Ming Ho

Michael Alan Teitell

Yong Chen

Pei-Yu Chiou, Committee Chair

University of California, Los Angeles

2016

# TABLE OF CONTENTS

# Yu-Chun Kung

## EDUCATION

**M.S., Electrical Engineering** **June 2007**
**National Taiwan University, Taipei, Taiwan** **GPA : 4.0/4.0**
**Advisor : Kuen-Yu Tsai and Ying-Chih Chang**

**B.S., Mechanical Engineering** **June 2005**
**National Taiwan University, Taipei, Taiwan** **GPA: 3.8/4.0**

## SKILLS

**Analytical Related**

- Electrokinetics, semiconductor physics , microfluidics, fluid mechanics, optics, mechatronics

**Microfabrication Related**

- Photolithography, e-beam evaporation, LPCVD, PECVD, wet etching(isotropic and anisotropic), dry etching(isotropic: RIE and anisotropic: DRIE)
- 3D PDMS Soft lithography, Hot-Embossing
- Laser machining(CW laser and Pulsed laser)
- SEM, AFM, microscopy

**Programming Related**

- MATLAB, Simulink, COMSOL Multiphysics, C/C++, Labview, AutoCAD, Solidworks, CoventorWare, OrCAD, TSUPREM-4, MEDICI

**Language**

- Fluent in English and Mandarin

## WORKING EXPERIENCES

**Graduate Student Researcher** **Sep. 2010-present**
Mechanical Engineering, University of California, Los Angeles, USA

- High-speed, high-throughput dielectrophoresis-based cell/bacteria sorter
- High-throughput, on-demand droplet microfluidics

**Device Development Engineer** **Jun. 2013-present**
NantBioScience, Los Angeles, USA

- High-throughput rare cell sorting (CTC) technology
- High-throughput drug screening technology

**Teaching Assistant** **Sep. 2013-Dec. 2013**
Mechanical Engineering, University of California, Los Angeles, USA

- Microfabrication process
- Microfluidics

## HONORS AND AWARDS

**Dissertation Year Fellowship**, UCLA **July 2015-June 2016**
**Mechanical and Aerospace Research Fellowship**, UCLA **Sep. 2010-June 2011**
**Presidential Award x 2**, National Taiwan University **Sep. 2006-June 2007**
**Presidential Award x 3**, National Taiwan University **Sep. 2003-June 2005**
**OKWAP Scholarship**, Inventec Appliances Corporation **Sep. 2004-June 2005**

## PUBLICATIONS

**Journals:**

1. Y.-C. Kung, K.-W. Huang, Y.-J. Fan, and P.-Y. Chiou, "Fabrication of 3D High Aspect Ratio PDMS Microfluidic Networks with A Hybrid Stamp", Lab on a Chip, Vol. 15(8), pp. 1861 – 1868, **2015**.
2. Y.-J. Fan,Y.-C. Wu, Y. Chen, Y.-C. Kung, T.-H. Wu, K.-W. Huang, H.-J. Sheen, and P.-Y. Chiou, "Three dimensional microfluidics with embedded microball lenses for parallel and high throughput multicolor fluorescence detection", Biomicrofluidics, **7**, 044121, **2013**.
3. Y. Chen, T.-H. Wu, Y.-C. Kung, Michael A. Teitell, and P.-Y. Chiou, "3D pulsed laser-triggered high-speed microfluidic fluorescence-activated cell sorter", Analyst, 138, 7308-7315, **2013**.

**Conference Proceedings:**

1. Y.-C. Kung and P.-Y. Chiou, "Tunable, High-Speed, and 3D Microfluidic Device for Ultra-High Precision Size-Based Particle Separation", Proceeding of the 29th IEEE International Conference on. Micro Electro Mechanical Systems, **2016**.
2. Y.-C. Kung, W. Chong, and P.-Y. Chiou, "Tunable, Sheathless, and Three Dimensional Single-Stream Cell Focusing in High Speed Flows", Proceeding of the 19th International Conference on Miniacturized Systems for Chemistry and Life Sciences, **2015**.
3. Y.-C. Kung, D. Clemens, B.-Y. Lee, and P.-Y. Chiou, "Tunable Dielectrophoresis for Sheathless 3D Focusing", Proceeding of the 28th IEEE International Conference on Micro Electro Mechanical Systems, **2015.**
4. Y.-C. Kung, K.-W. Huang, and P.-Y. Chiou, "Flow-decoupled dielectrophoresis for sheathless 3D focusing in high speed flows", Proceeding of the 18th International Conference on Miniacturized Systems for Chemistry and Life Sciences, **2014**.
5. K.-W. Huang, Y.-C. Kung, Y.-C. Wu, Y.-J. Fan, and P.-Y. Chiou, "Optoelectronic Tweezers Integrated with 3D Microfluidic Networks", 2013 International Conference on Optical MEMS and Nanophotonics, **2013**.
6. Y.-J. Fan, Y. Chen, Y.-C. Wu, Y.-C. Kung, T.-H. Wu, H.-J. Sheen, and P.-Y. Chiou, "Multicolor ultra high throughput parallel microfluidic flow cytometer", Proceeding of the 17th International Conference on Solid State Sensors and Actuators, **2013**.
7. Y. Chen, T.-H. Wu, Y.-C. Kung, Michael A. Teitell, and P.-Y. Chiou, "3D pulsed laser triggered high speed microfluidic fluorescence activated cell sorter", Proceeding of the International Conference on Lasers and Electro Optics, **2013**.
8. Y.-C. Kung, K.-W. Huang, Y. Yang., Y.-J. Fan, and P.-Y. Chiou, "Fabrication of 3D microfluidic networks with A hybrid stamp", Proceeding of the 26th International Conference on Micro Electro Mechanical Systems, **2013**.
9. Y. Chen, T.-H. Wu, Y.-C. Kung, and P.-Y. Chiou, "3D pulsed laser triggered high speed microfluidic fluorescence activated cell sorter", Proceeding of the 16th International Conference on Miniacturized Systems for Chemistry and Life Sciences, **2012**.
10. Y.-J. Fan, Y.-C. Kung, Y.-C. Wu, K.-W. Huang, T.-H. Wu, Y. Chen, H.-J. Sheen, and P.-Y. Chiou, "High throughput fluorescence based flow cytometer using 3D microfluidics for parallel sheath flow focusing and embeded high N.A. microlens", Proceeding of the 16th International Conference on Miniacturized Systems for Chemistry and Life Sciences, **2012**.

# CHAPTER 1

## INTRODUCTION

### 1.1 Introduction of Bio-Microsystems

The development of lab-on-a-chip (LOC) devices over the past decade has attracted growing interest. LOC devices aim to achieve the miniaturization, integration, automation and parallelization of biological and chemical assays. One of the applications, the ability to effectively and accurately manipulate and separate micro- and nano-scale particles in an aqueous solution, is particularly appealing in biological, chemical and medical fields. [1] Their small volume reduces the time required to synthesize and analysis. In addition, compact devices have been able to achieve massive parallelization and high-throughput analysis. [2] Meanwhile, the lower fabrication costs contribute to the mass production of disposable chips. The features of compactness, portability, sensitivity and parallelization make LOC devices beneficial for various applications, including point-of-care (POC) diagnostics [3], drug delivery [4], molecule and material synthesis [5], chemical reaction control and detection [6], and cellular process studies [7]. One existing application of LOC devices is to manipulate and separate particles (both synthetic and biological), which plays an important role in the field of biology, chemistry and medicine.

To date, a variety of technologies have been developed to manipulate and separate particles in an aqueous solution, including mechanical, inertial, hydrodynamic, acoustic, optical, magnetic and electrical methodologies [8]. Among these available methods, dielectrophoresis (DEP) has attracted most attention due to its considerable advantages [9]. Unlike other techniques, DEP depends on the dielectric properties, which represent the structural, morphological and chemical characteristics of bioparticles, allowing highly selective and sensitive analysis [10]. DEP manipulation is straightforward and fully controllable by varying the electric conductivity of the suspending medium or the frequency and magnitude of the electric field applied. DEP is also easily and directly interfaced to conventional electronics, and can be used in the fabrication of LOC devices. In addition, DEP enables contact-free manipulation of particles (both charged and neutral) with lower sample consumption and fast speed [11]. DEP is a phenomenon that occurs due to a translational force exerted on a dielectric particle in a non-uniform electric field. A dielectric particle and the suspending medium become electrically polarized in an electric field, which separates the electric charge at the interface between solid and liquid. Depending on the relative polarizability of the particle and suspending medium, a net dielectrophoretic force will attract the particle towards the region of higher electric field gradient (positive

DEP) or push the particle towards the region of lower electric field gradient (negative DEP). DEP has proven to be a versatile mechanism for manipulating various micro/nano-scale bioparticles (i.e. cells, viruses, bacteria, DNA and proteins) in microfluidic systems.

Two main methods are used to generate the electric field gradient that is required for the DEP effect, which are: microelectrodes and insulator structures. Traditionally, high-frequency alternating current (ac) electric fields were applied via two-dimensional (2D) or three-dimensional (3D) microelectrode arrays embedded within the microchannels [11]. The 2D planar microelectrodes were normally patterned on the bottom floor of the microchannel by the photolithograph, thin-film deposition and lift-off techniques, which could affect the movement of particles close to the surface of the electrode [12]. Alternatively, 3D microelectrode structures (such as extruded vertical electrodes on the bottom , top–bottom patterned, and sidewall-patterned microelectrodes) have been developed and fabricated using more complicated techniques (i.e. electroplating and pyrolysis), which can generate DEP forces over a larger volume within the microchannel [12]. Alternatively, inhomogeneous electric fields can be induced by insulator structures [13] that are normally fabricated by the soft lithograph technique, in which either insulating obstacles are embedded within the microchannel or the geometry of the insulating

microchannel is modified while direct current (dc) or dc biased low-frequency ac electric fields are applied via external electrodes placed in the inlet and outlet reservoirs. The microfabrication techniques currently available have been applied to build electrodeand insulator-based dielectrophoretic microdevices. With the rapid development of LOC or μTAS in recent years, various microfabrication techniques have been developed and applied for dielectrophoretic applications. Consequently, dielectrophoretic microdevices with different configurations and structures of microelectrodes and insulators have been successfully used to manipulate and separate particles.

To summarize, DEP has proven to be a versatile mechanism for manipulating various micro/nano-scale bioparticles (i.e. cells, viruses, bacteria, DNA and proteins) in microfluidic systems, but lack of general fabrication and design platform for 3D and massively parallel capabilities for high throughput applications. In this dissertation, I propose a novel fabrication method, which can achieve heterogeneous integration between PDMS and hard substrates with electronics. This novel fabrication and design platform permits 3D electric field generated across the whole device, which enables manipulation of particles or cells three-dimensionally in high-speed flows. Details of the applied mechanisms are discussed in the following sessions.

## 1.2 Particle Manipulation techniques

Manipulating and separating particles is a critical activity in a variety of biological, medical and biochemical applications. However, traditional techniques are labour intensive, and require multiple additional tags or labels to identify target particles. Fluorescence-activated cell sorting (FACS) [14] and magnetic-activated cell sorting (MACS) [15] utilize fluorophore-conjugated antibodies and magnetic beads conjugated with antibodies to label the cells of interest, respectively. Although both methods offer high-throughput screening with rich data outputs, they are costly in terms of system setup, operation and reagent consumption. Moreover, centrifugation is a common technique to separate particles in bulk, based on their differences in size and density [16]; however, this manual, macroscale, multistep technique needs laboratories dedicated to these functions and may introduce contamination during the process. Recently, interest has been expressed in label-free techniques that take advantage of the intrinsic properties of particle populations (such as size, shape, electrical polarizability and density) to accomplish particle/cell manipulation and separation in fluid, which involve mechanical, inertial, hydrodynamic, acoustic, optic, magnetic and electrical methodologies.

1) The mechanical manipulation of bioparticles (i.e. blood cells [17], plasma [18] and circulating tumour cells (CTCs) [19]) based on size has been achieved by fabricating constriction structures (i.e. weir [20] and pillar [21]) within the microchannels. Although these filter-based microfluidic devices have several advantages (such as high labelling efficiency and reproducibility), there are many challenges to their use, including: the heterogeneity of cell sizes within a population, clogging, fouling and limited selectivity for biological assays.
2) Inertial lift forces acting on particles in high-velocity flows have been utilized to manipulate polystyrene particles, cells and bacteria within various-shaped microchannels, such as curved [22], asymmetrically curved [23], spiral microchannels [24], a microchannel consisting of a focusing, an expansion and collection region [25]. Inertial separation offers high volumetric flow rates but requires dilution (either prior to injection or within the device) to eliminate particle–particle interactions and lack of precise particle manipulation spatial resolution nonetheless for biological cells.
3) The acoustic technique is based on the concept that particles suspended in a fluid experience an acoustic radiation force when they are exposed to an ultrasound. There are several reports regarding the application of an ultrasonic standing wave field

combined with laminar flow to separate different-sized particles [26], 2D array patterning [27], and sheathless single-stream focusing [28].

4) Optical tweezers could tether biological molecules to particles and then capture the particles at the focal point of an electric field gradient, which has been widely used as a tool for the manipulation and trapping of particles [29]. However, its application in microfluidics is still limited due to the weak attractive force, complicated setup, complex operation and expensive instrumentation.
5) Magnetic manipulation is a passive and label-based method that achieved by selectively bonding cells with magnetic beads, and then separating them by applying a magnetic field. In addition, the intrinsic magnetophoretic properties of particles or cells (or magnetophoresis) have been employed for separation and purification. The separation of red and white blood cells (WBCs) from whole blood [30], and CTCs sorting [31].
6) Two main kinds of electrical force have been well used to manipulate particles; that is, the electrophoretic force and the dielectrophoretic force. Electrophoretic force is a kind of electrostatic Coulomb force that is generated by the interaction between the net surface charge on the particle and the applied electric field. The induced movement of the charged particle relative to a fluid is known as electrophoresis

(EP). Several studies have demonstrated the biological applications of EP, and have been reviewed by [32]. However, for biological particles that are electrically neutral, EP may not applicable due to the absence of net charge, whereas a DEP force that arises from the interaction between the particle's dipole and a non-uniform electric field can be used to manipulate neutral particles. With the recent rapid development of LOC devices, DEP has been widely used for particle sorting, focusing, patterning and positioning due to its many advantages.

## 1.3 Dielectrophoresis (DEP)

Having chosen dielectrophoresis (DEP) as the trapping force, in this section I will describe the physics behind this phenomenon and give an overview of the field.

DEP refers to the action of a body in a non-uniform electric field when the body and the surrounding medium have different polarizabilities. DEP is easiest illustrated with reference to Figure 1-1. On the left side of Figure 1-1, a charged body and a neutral body (with different permittivity than the medium) are placed in a uniform electric field. The charged body feels a force, but the neutral body, while experiencing a dipole moment, does not feel a net force. This is because each half of the induced dipole feels opposite and equal forces,

which cancel. On the right side of Figure 1-1, this same body is placed in a non-uniform electric field. Now the two halves of the induced dipole experience a different force magnitude and thus a net force is produced. This is the dielectrophoretic force.

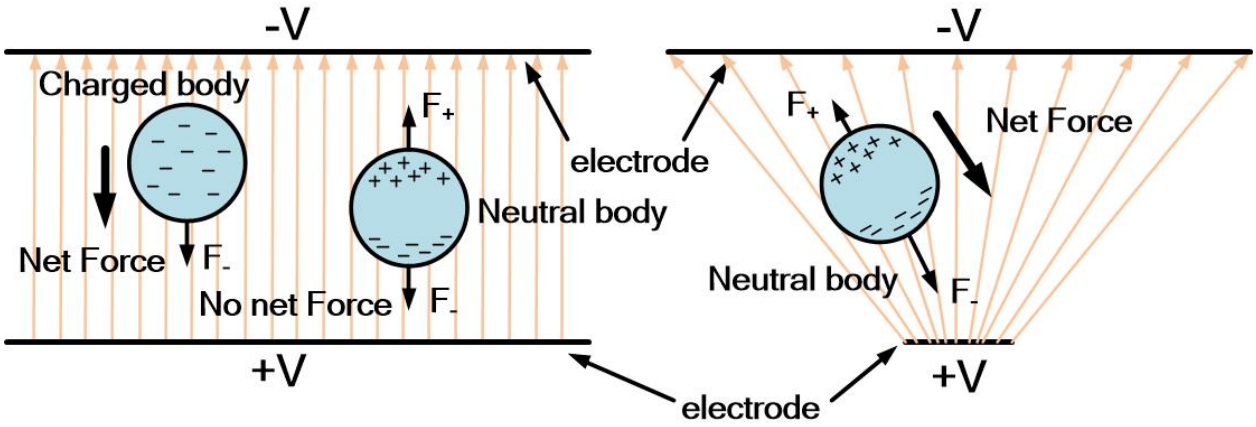


Figure 1-1 Dielectrophoresis. The left panel shows the behavior of particles in uniform electric fields, while the right panel shows the net force experienced in a non-uniform electric field.

Depending on the relative polarizabilities of the particle and the medium, the body will feel a force that propels it toward field maxima (termed positive DEP) or field minima (negative DEP). In addition, the direction of the force is independent of the polarity of the applied voltage; switching the polarity of the voltage does not change the direction of the force—it is still towards the field maximum. Thus DEP works equally well with both DC and AC fields. DC and AC fields.

DEP should be contrasted with electrophoresis, where one manipulates charged particles in a dissipative medium with electric fields, as there are several important differences. First, DEP does not require the particle to be charged in order to manipulate it; the particle must only differ electrically from the medium that it is in. Second, DEP works with AC fields, whereas no net electrophoretic movement occurs in such a field. Thus, with DEP one can avoid problems such as electrolysis at electrodes. Even more importantly, the use of AC fields reduces membrane charging of biological cells. Membrane charging is due to the potential developed across cell membranes in electric fields. This potential, which can impact cell physiology, can be diminished by the application of high-frequency fields. Third, electrophoretic systems cannot create stable traps, as opposed to DEP—one needs electromagnetic fields to trap charges. Finally, DEP forces increase with the square of the electric field (described below), whereas electrophoretic forces increase linearly with the electric field.

The force in Figure 1-1, where an induced dipole is affected by a non-uniform electric field, is given by

$$F_{DEP} = 2\pi\varepsilon_m R^3 Re[\overline{CM}(\omega) \cdot \nabla|\bar{E}|^2(r)] \qquad (1\text{-}1)$$

where $\varepsilon_m$ is the permittivity of the medium surrounding the particle, *R* is the radius of the particle, $\omega$ is the radian frequency of the applied

field, *r* refers to the spatial coordinate, and *E* is the complex applied electric field.

The Clausius-Mossotti factor ( $\overline{CM}$ )—CM factor—gives the frequency ($\omega$) dependence of the force, and its sign determines whether the particle experiences positive or negative DEP. For a homogeneous spherical particle in an electric field, the CM factor is given by

$$\overline{CM} = \frac{\overline{\varepsilon_p} - \overline{\varepsilon_m}}{\overline{\varepsilon_p} + 2\overline{\varepsilon_m}} \tag{1-2}$$

where $\overline{\varepsilon_m}$ and $\overline{\varepsilon_p}$ are the complex permittivities of the medium and the particle, respectively, and are each given by $\bar{\varepsilon} = \varepsilon + \sigma/(j\omega)$, where $\varepsilon$ is the permittivity of the medium or particle, $\sigma$ is the conductivity of the medium or particle, and j is $\sqrt{-1}$.

The Clausius-Mossotti factor of a particle represents its frequency response to an external electric field. It is the particle's dielectric signature, which characterizes the particle's size, composition, structure, and surface charge concentration. For a spherical particle with single shell, each cytoplasma and cell membrane with different dielectric constant and conductivity, as shown in Figure 1-2, the CM factor can be derived from an equivalent complex permittivity as

$$\overline{CM}\left(\varepsilon_p', \varepsilon_m\right) = \frac{\overline{\varepsilon_{p'}} - \overline{\varepsilon_m}}{\overline{\varepsilon_{p'}} + 2\overline{\varepsilon_m}} \quad (1\text{-}2)$$

$$\overline{\varepsilon_p'} = \overline{\varepsilon_2}\left[\frac{a^3 + 2\left(\frac{\overline{\varepsilon_3} - \overline{\varepsilon_2}}{\overline{\varepsilon_3} + 2\overline{\varepsilon_2}}\right)}{a^3 - \left(\frac{\overline{\varepsilon_3} - \overline{\varepsilon_2}}{\overline{\varepsilon_3} + 2\overline{\varepsilon_2}}\right)}\right] \quad (1\text{-}3)$$

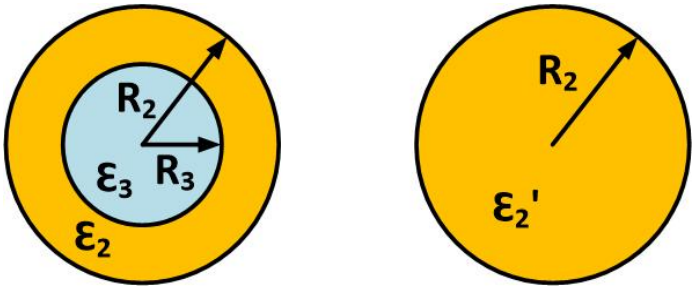


Figure 1-2 Spherical dielectric shells with radii of $R_2$ and $R_3$ of shell and cytoplasma, and permittivities of $\varepsilon_2$ and $\varepsilon_3$, respectively.

where $\overline{\varepsilon_2}$ and $\overline{\varepsilon_3}$ are the complex permittivities of the medium and the shells of the particle, $a=R_2/R_3$, and $\overline{\varepsilon_{p'}}$ is the new equivalent permittivity of the particle. The real part of $\overline{CM}$, Re[$\overline{CM}$], has a value between 1 and –1/2, depending on the polarizability of the medium and the particle at a certain frequency. If Re[$\overline{CM}$] >0, the induced electric dipole is collinear with the electric field as shown in Figure 1-3(b). The particle will move towards the strong electric field region, a phenomenon known as positive DEP. On the other hand, if Re[$\overline{CM}$] <0, the induced electric dipole is anti-parallel to the electric field as shown in Figure 1-3(a). The particle moves towards the weaker electric field region, known as negative DEP.

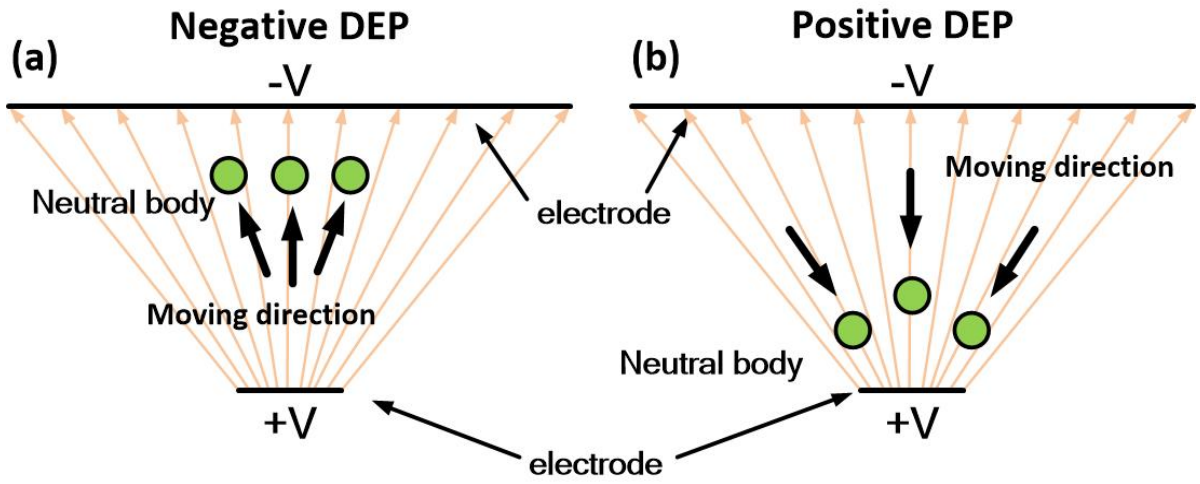


Figure 1-3 Illustration of positive and negative DEP forces. (a) For positive DEP, the field induced electric dipole on the particle is collinear with the direction of the applied electric field. The particles move towards the strong electric field region. (b) For negative DEP, the dipole direction is anti-parallel to the applied electric field and the particles are pushed towards the weaker electric field region.

Thus, similar to many electroquasistatic systems, the CM factor will be dominated by relative permittivities at high frequency and conductivities at low frequencies; the induced dipole varies between a free charge dipole and a polarization dipole. The relaxation time separating the two regimes is

$$\tau_{MW} = \frac{\varepsilon_p + 2\varepsilon_m}{\sigma_p + 2\sigma_m} \tag{1-4}$$

and is denoted $\tau_{MW}$ to indicate that the physical origin is Maxwell-Wagner interfacial polarization.

Figure 1-4 shows the frequency-dependent values of the real part of the CM factor of a simulated mammalian cell in various medium conductivities. In order to simulate the cell using Equ. (1-1), the cell is represented by a simple dielectric model. Two types of cells, THP1 and HeLa cells are used for the simulation with corresponding sizes of 10μm and 15μm in diameter. The cell membrane is formed by a lipid bilayer and has a thickness around 10 nm. In a live cell, this membrane is selectively permeable to ions and can be modeled as a low conductivity layer. Inside the cell membrane are the subcellular structures and cytoplasm, which consist of ions, proteins, and sugars. The average liquid conductivity inside the cell membrane is assumed to be 0.5 S/m.

At low frequencies (Figure 1-4(a)), the real-part of the CM factor is negative, meaning the induced DEP force is negative. In this range, the cell membrane is fully charged with ions, and a large electric field across the membrane can rupture the cell. When the applied frequency increases, the real part of the CM factor starts to move to positive regime, as the ions in the medium do not have time to charge the membrane capacitance The frequency at which the real part of the CM factor begins to increase is characterized by the time constant $\tau_1$ =

$RC_{mem}/\sigma_m$, where $R$ is the radius of the cell, $C_{mem}$ is the cell membrane capacitance, and $\sigma_m$ is the medium conductivity outside the cell membrane. For a 0.01 S/m medium conductivity, this transition starts at 20 kHz. At 60 kHz, the electrical impedance of the membrane capacitance is comparable to the liquid medium, resulting in the real part of the CM factor having a value of zero. This frequency is called cross-over frequency, and no DEP force is induced. As the frequency is increased further, the real part of the CM factor saturates at a constant value, which is determined by the conductivity terms of the media in the cell interior and outside the cell membrane, $(\sigma_c - \sigma_m)/(\sigma_c + 2\sigma_m)$, where $\sigma_c$ and $\sigma_m$ are the conductivity of the cytoplasm and the extracellular medium, respectively. If the medium is less conductive than the cell, this value will be positive; on the other hand, if the medium is more conductive, the value at higher frequencies would be negative, and the cell does not have a positive DEP regime, as seen in the 1 S/m curve of Fig. 1-4(b).

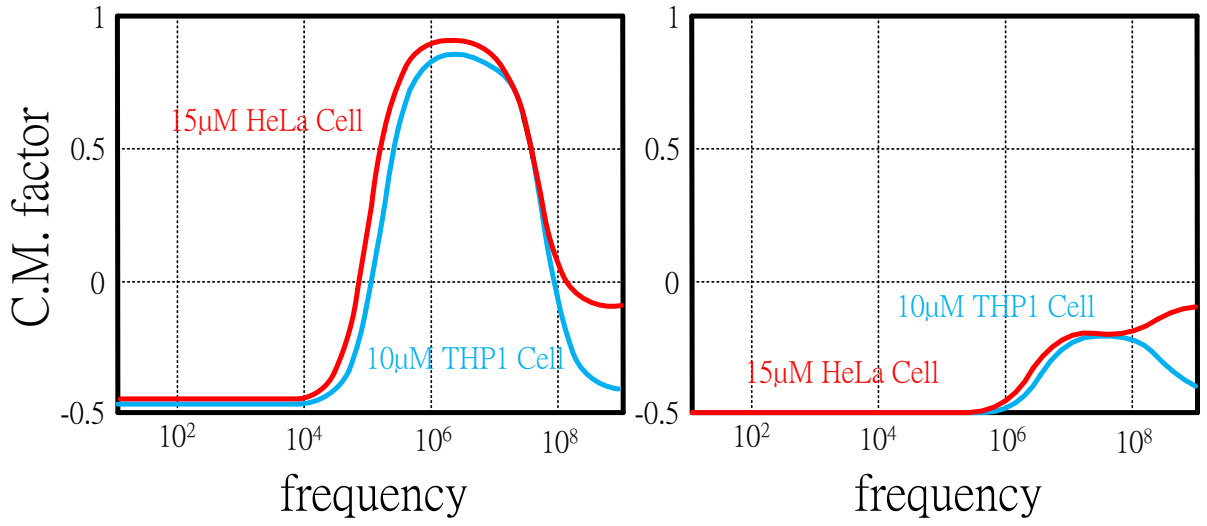


Figure 1-4 The simulated real part CM factor of THP1 (10μm in diameter) and HeLa (15μm in diameter) cells in mediums with liquid conductivities of 0.01 S/m and 1 S/m. The cell membrane is assumed to have a 10 nm thickness and a low conductivity. Inside the cell membrane, the liquid conductivity is assumed to have a constant value of 0.5 S/m.

## 1.4 Reference


1. Lim, Y.C., A.Z. Kouzani, and W. Duan, *Lab-on-a-chip: a component view.* Microsystem Technologies, 2010. **16**(12): p. 1995-2015.
2. Trietsch, S.J., T. Hankemeier, and H.J.v.d. Linden, *Lab-on-a-chip technologies for massive parallel data generation in the life sciences: A review.* Chemometrics and Intelligent Laboratory Systems, 2011. **108**(1): p. 64-75.
3. Schumacher, S., et al., *Highly-integrated lab-on-chip system for point-of-care multiparameter analysis.* Lab on a Chip, 2012. **12**(3): p. 464-473.
4. Nguyen, N.-T., et al., *Design, fabrication and characterization of drug delivery systems based on lab-on-a-chip technology.* Advanced Drug Delivery Reviews, 2013. **65**(11): p. 1403-1419.
5. Günther, A. and K.F. Jensen, *Multiphase microfluidics: from flow characteristics to chemical and materials synthesis.* Lab on a Chip, 2006. **6**(12): p. 1487-1503.
6. Zhao, Y., et al., *Lab-on-a-chip technologies for single-molecule studies.* Lab on a Chip, 2013. **13**(12): p. 2183-2198.

7. Mohammed, M.-I. and M.P.Y. Desmulliez, *Lab-on-a-chip based immunosensor principles and technologies for the detection of cardiac biomarkers: a review.* Lab on a Chip, 2011. **11**(4): p. 569-595.
8. IV, C.W.S., C.D. Reyes, and G.P. López, *Microfluidic cell sorting: a review of the advances in the separation of cells from debulking to rare cell isolation.* Lab on a Chip, 2015. **15**(5): p. 1230-1249.
9. Hughes, M.P., *Strategies for dielectrophoretic separation in laboratory-on-a-chip systems.* Electrophoresis, 2002. **23**(16): p. 2569-2582.
10. Pysher, M.D. and M.A. Hayes, *Electrophoretic and dielectrophoretic field gradient technique for separating bioparticles.* Analytical Chemistry, 2007. **79**(12): p. 4552-4557.
11. Zhang, C., et al., *Dielectrophoresis for manipulation of micro/nano particles in microfluidic systems.* Analytical and Bioanalytical Chemistry, 2010. **396**(1): p. 401-420.
12. Khoshmanesh, K., et al., *Dielectrophoretic platforms for bio-microfluidic systems.* Biosensors and Bioelectronics, 2011. **26**(15): p. 1800-1814.
13. Regtmeier, J., et al., *Electrodeless dielectrophoresis for bioanalysis: Theory, devices and applications.* Electrophoresis, 2011. **32**(17): p. 2253-2273.
14. Davey, H.M. and D.B. KEell, *Flow Cytometry and Cell Sorting of Heterogeneous Microbial Populations: the Importance of Single-Cell Analyses.* MICROBIOLOGICAL REVIEWS, 1996. **60**(4): p. 641-696.
15. Miltenyi, S., et al., *High gradient magnetic cell separation with MACS†.* Cytometry, 1990. **11**(2): p. 231-238.
16. Leung, W.W.-F., *Centrifugal Separations in Biotechnology*. 2007: Oxford.
17. VanDelinder, V. and A. Groisman, *Perfusion in Microfluidic Cross-Flow: Separation of White Blood Cells from Whole Blood and Exchange of Medium in a Continuous Flow.* Analytical Chemistry, 2007. **79**(5): p. 2023-2030.
18. VanDelinder, V. and A. Groisman, *Separation of Plasma from Whole Human Blood in a Continuous Cross-Flow in a Molded Microfluidic Device.* Analytical Chemistry, 2006. **78**(11): p. 3765-3771.
19. Zheng, S., et al., *Membrane microfilter device for selective capture, electrolysis and genomic analysis of human circulating tumor cells.* Journal of Chromatography A, 2007. **1162**(2): p. 154-161.
20. Wilding, P., et al., *Integrated Cell Isolation and Polymerase Chain Reaction Analysis Using Silicon Microfilter Chambers.* Analytical Biochemistry, 1998. **257**(2): p. 62-100.
21. Mohamed, H., J.N. Turner, and M. Caggana, *Biochip for separating fetal cells from maternal circulation.* Journal of Chromatography A, 2007. **1162**(2): p. 187-192.
22. Gossett, D.R. and D.D. Carlo, *Particle Focusing Mechanisms in Curving Confined Flows.* Analytical Chemistry, 2009. **81**(20): p. 8459-8465.
23. Carlo, D.D., et al., *Continuous inertial focusing, ordering, and separation of particles in microchannels.* Proceedings of the National Academy of Sciences of the United States of America, 2007. **104**(48): p. 18892-18897.
24. Kuntaegowdanahalli, S.S., et al., *Inertial microfluidics for continuous particle separation in spiral microchannels.* Lab on a Chip, 2009. **9**(20): p. 2973-2980.
25. Mach, A.J. and D.D. Carlo, *Continuous scalable blood filtration device using inertial microfluidics.* Biotechnology and Bioengineering, 2010. **107**(2): p. 302-311.
26. Petersson, F., et al., *Free Flow Acoustophoresis: Microfluidic-Based Mode of Particle and Cell Separation.* Analytical Chemistry, 2007. **79**(14): p. 5117-5123.
27. Ding, X., et al., *On-chip manipulation of single microparticles, cells, and organisms using surface acoustic waves.* Proceedings of the National Academy of Sciences of the United States of America, 2012. **109**(28): p. 11105-11109.

28. Chen, Y., et al., *Standing surface acoustic wave (SSAW)-based microfluidic cytometer.* Lab on a Chip, 2014. **14**(5): p. 916-923.
29. Wang, M.M., et al., *Microfluidic sorting of mammalian cells by optical force switching.* Nature Biotechnology, 2005. **23**: p. 83-87.
30. Jung, J. and K.-H. Han, *Lateral-driven continuous magnetophoretic separation of blood cells.* Applied Physics Letters, 2008. **93**(22): p. 223902.
31. Karabacak, N.M., et al., *Microfluidic, marker-free isolation of circulating tumor cells from blood samples.* Nature Protocols, 2014. **9**: p. 694-710.
32. Korohoda, W. and A. Wilk, *Cell electrophoresis — a method for cell separation and research into cell surface properties.* Cellular and Molecular Biology Letters, 2008. **13**(2): p. 312-326.
33. Gao, J., et al., *Electrokinetic focusing and separation of mammalian cells in conductive biological fluids.* Analyst, 2012. **137**(22): p. 5215-5221.
34. Han, K.-H. and A.B. Frazierb, *Lateral-driven continuous dielectrophoretic microseparators for blood cells suspended in a highly conductive medium.* Lab on a Chip, 2008. **8**(7): p. 1079-1086.
35. Hu, X., et al., *Marker-specific sorting of rare cells using dielectrophoresis.* Preceedings of the National Academy of Sciences of the United States of America, 2005. **102**(44): p. 15757-15761.
36. Kim, U., et al., *Multitarget Dielectrophoresis Activated Cell Sorter.* Analytical Chemistry, 2008. **80**(22): p. 8656-8661.
37. Kim, U., et al., *Selection of mammalian cells based on their cell-cycle phase using dielectrophoresis.* Preceedings of the National Academy of Sciences of the United States of America, 2007. **104**(52): p. 20708-20712.

# CHAPTER 2

## FABRICATION OF 3D HIGH ASPECT RATIO PDMS MICROFLUIDIC NETWORKS WITH A HYBRID STAMP

### 2.1. Abstract

We report on a novel methodology for fabricating large-area, multilayer, thin-film, high aspect ratio, 3D microfluidic structures with through-layer vias and open channels that can be bonded between hard substrates. It is realized by utilizing a hybrid stamp with a thin plastic sheet embedded underneath a PDMS surface. This hybrid stamp solves an important edge protrusion issue during PDMS molding process while maintaining necessary stamp elasticity to ensure the removal of PDMS residues at through-layer regions. Removing edge protrusion is a significant progress toward fabricating 3D structures since high aspect ratio PDMS structures with flat interfaces can be realized to facilitate multilayer stacking and bonding with hard substrates. Our method also allows for the fabrication of 3D deformable channels, which can lead to profound applications in electrokinetics, optofluidics, inertial microfluidics, and other fields where the shape of channel cross-section plays a key role in device physics. To demonstrate, as an example, we have fabricated a microfluidic channel by sandwiching two 20 μm wide, 80 μm tall PDMS

membranes between two featureless ITO glass substrates. By applying an electrical bias to the two ITO substrates and a pressure to deform the thin membrane sidewalls, strong electric field enhancement can be generated in the center of a channel to enable 3D sheathless dielectrophoretic focusing of biological objects including mammalian cells and bacteria at a flow speed up to 14 cm/sec.

## 2.2. Introduction

Lab on a chip systems have attracted tremendous interests in both academics and industries in the past decade for their potential applications in personal medicine, health care, environmental monitoring, and chemical synthesis [1]. With the increasing demand of more integrated functions on a chip, advancements in manufacturing technology are critical to provide flexibility on integration of heterogeneous materials, a better interface between macro and micro components, and simple routing approaches for massively parallel fluid manipulation and control. 3D microfluidics is one of the future trends since it not only significantly increases the number of functional units that can be integrated on a chip, thus increasing the processing power and throughput, but also provides many important unique functions that are difficult to realize with conventional 2D technologies [2-4],

such as 3D sheath flows for sample focusing [5, 6] and 3D tissue engineering[7-14].

Versatile approaches have been demonstrated in prior literatures for fabricating 3D microfluidic structures. Silicon-based microfabrication allows the creation of high-resolution, high aspect ratio structures on silicon substrates, high conductivity metal electrodes for electrical sensing and actuation, and high quality semiconductor devices for IC integration. The drawbacks, however, are the high manufacturing costs and challenges to integrate with other microfluidic components. Thermal plastic hot embossing is a fast and efficient way for fabricating microfluidic structures[15]. Yet, it has residual membrane issues and cannot be used to fabricate uniform through-layer structures for interlayer communication. Photosensitive epoxy polymers such as SU-8 can be optically patterned and stacked through thermal bonding [16-18]. However, it is well known that during the spin-coating process, uneven thickness around the structures can hinder uniform bonding across a large area, which potentially leads to fluid leak.

Multilayer soft lithography (MSL) has been widely applied for fabricating microfluidic devices in the recent decade [19]. Numerous PDMS based devices from simple monolayer PDMS channels to complex multilayer microfluidic systems with pneumatically controlled pumps and valves have been demonstrated [20]. Thousands of valves

and chambers can be integrated on a chip to perform multistep biochemical analyses [21]. Most PDMS based devices, however, are not true 3D devices since they do not have through-layer structures such as holes or channels for vertical fluid routing. This limitation comes from the lack of a reliable approach for fabricating through-layer structures with high resolution. Without interlayer communication structures, fluid routing, control, and sample addressing become challenges when sample size becomes large.

Several prior fabrication approaches have been demonstrated to solve the issue of fabricating interlayer communication structures, but with different degrees of success. One simple method is the use of a multilevel mold with raised post structures. By spinning a thin, uncured PDMS layer on this mold, through-layer vias can be formed at locations with these raised posts [22]. This method, although simple, does not provide large area uniformity since it is sensitive to many parameters such as via height, membrane thickness, and density of vias. To prevent the formation of residual membranes at via locations, an approach utilizing pressure gas to blow off uncured PDMS at via locations has been demonstrated as well, but there are concerns regarding the throughput and uniformity across the chip.[23].

Another approach is to utilize a soft PDMS stamp to fabricate PDMS thin films with through-layer structures and stack them layer-by-layer

[24]. A soft PDMS stamp ensures the removal of the interface residues between the stamp and the mold. This approach, however, introduces an edge protrusion issue near vias due to a deformed stamp in the molding process. These nonplanar features can accumulate and limit the number of layers that can be stacked since bonding nonflat surfaces is challenging. For fine features such as narrow high-aspect-ratio structures, these protruding edges prohibit their bonding with hard substrates, and limit the structure resolution that can be fabricated. Another approach utilizing a hard glass stamp with the aid of amine surface treatment has also been demonstrated. The amine treatment can inhibit the polymerization process of a thin uncured PDMS layer adjacent to the stamp surface to remove the residual PDMS at through-layer regions [25, 26]. The diffusion-based polymerization inhibition process, however, limits the structure density and resolution of layer thickness. Another approach using CO2 laser to directly ablate through a thin PDMS film is also demonstrated. However, this approach generates rough surfaces and non-vertical sidewalls [27].

Here, we demonstrate a hybrid stamp approach to solve the edge protrusion issue and provide a reliable method for fabricating high aspect ratio (HAR), high resolution PDMS 3D thin-film structures across a large area. HAR is defined as the ratio of structure height to width. In this approach, a PDMS stamp is embedded with a thin plastic plate

underneath a chemically treated PDMS surface. This plastic plate increases the mechanical stiffness near the stamp surface to prevent severe deformation to eliminate the occurrence of protruding edges. A thin layer of elastic PDMS film on top of the plastic plate provides the required elasticity to ensure a complete removal of uncured PDMS residues at through-layer regions. Removing edge protrusion is a significant step. It permits the fabrication of high resolution, large area, high-aspect-ratio PDMS thin films with through-layer features to construct 3D microfluidic devices. Flat PDMS interfaces allow narrow HAR structures to be bonded reliably between hard substrates, on which high quality electronic, optical, and semiconductor devices are typically fabricated. This gives chip designers more flexibility in integrating heterogeneous materials, structures, devices, and systems on the same chip with more functional modules.

## 2.3. Fabrication of 3D Microfluidic Networks with a Hybrid Stamp

Figure 2-1 shows the schematic of the process flow of fabricating 3D microfluidic structures using the hybrid stamp approach.

**Step 1**: Fabrication of master molds. It starts from fabricating SU-8 mold masters on silicon wafers using photolithography (Figure 2-1 (a)). A thin SU-8 layer is coated before the thick SU-8 mold to enhance the adhesion to the bulk silicon wafer. All masters need to be surface

treated with trichloro (1H,1H,2H,2H-perfluorooctyl) silane (97%, Sigma-Aldrich, USA), also called PFOCTS, to facilitate later demolding. This surface treatment was carried out in a vacuum chamber at a pressure of -30 psi for 16 hours.

**Step 2**: Fabrication of hybrid stamps. It starts from preparing the Sylgard 184 silicone elastomer mixture (Dow Corning Corporation, Miland, USA). The ratio of Base : Curing agent is 10g : 1g. Few drops of this mixture are poured into a petri dish. A suitable size of polystyrene plastic plate is cut and pressed against the bottom of the petri dish under a pressure of 3 psi. A thin layer of polydimethylsiloxane (PDMS) with a thickness of roughly 30μm is formed between the petri dish and the plastic plate. Additional uncured PDMS is poured to fill up the petri dish, followed by a curing step at 600C in an oven for 12 hours. A hybrid stamp is formed when the plastic plate together with a thin PDMS layer on its surface is peeled off from the petri dish (Figure 2-1(b)). The hybrid stamp is also surface treated with PFOCTS as in Step 1 for 6 hours. To fabricate PDMS thin film with through-layer structures, uncured PDMS is poured onto the master mold, pressed by the hybrid stamp under a pressure of 4psi, and cured at 500C in an oven for an hour.

**Step 3**: Demolding PDMS films from master mold. During the demolding process, the cured PDMS thin film has stronger adhesion to

the hybrid stamp than to the master mold since more PFOCTS is coated on the master mold due to a longer treatment time (Figure 2-1(c)).

**Step 4**: Transfer and stack PDMS thin films. Oxygen plasma treatment is performed on both the PDMS thin film on the hybrid stamp and the substrate to be bonded for two minutes. Alignment is performed under a microscope before bonding (Figure 2-1(d)). The bonded set is baked in an oven at $60^0$C for 2 hours.

**Step 5**: Removing hybrid stamp. It starts from peeling off the bulk PDMS part on the plastic plate (Figure 2-1(e)), followed by dissolving the polystyrene plastic plate in an acetone bath for 4 hours (Figure 2-1(f)). This leaves a thin residual PDMS film on the substrate that can be easily peeled off from the device due to prior PFOCTS treatment (Figure 2-1(g)) to finish the transferring and stacking process of a PDMS thin film with through-layer structures. This mechanically gentle releasing technique allows us to transfer PDMS thin film to fragile substrates, such as a glass cover slip, over a large area.

**Step 6**: Constructing multilayer 3D microfluidic devices. By repeating step 1-5, multilayer 3D PDMS structures with interlayer vias and high aspect ratio structures could be constructed and bonded between two hard substrates (Figure 2-1(h)).

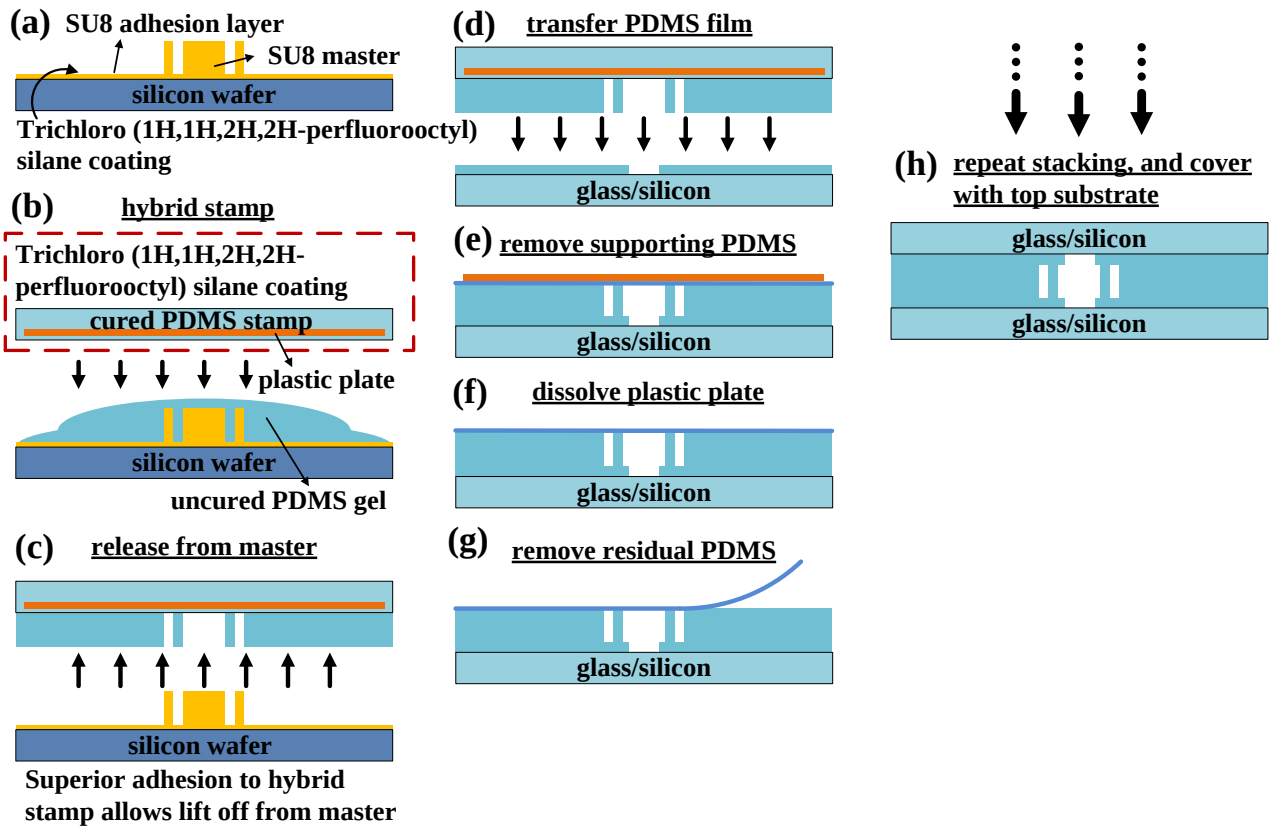


Figure 2-1 Schematic of fabrication process flow using a plastic plate embedded hybrid stamp. (a) A SU8 master is treated with PFOCTS to facilitate later demolding. (b) Uncured PDMS mixture is poured on the master, and pressed against the hybrid stamp. (c) Due to less PFOCTS treatment on the hybrid stamp compared to the master, the casted PDMS film tends to adhere to the hybrid stamp and allows to be peeled off from the master. (d) The film is transferred and bonded by oxygen plasma treatment (e) Remove the support PDMS on the hybrid stamp. (f) Dissolve the polystyrene plastic plate in acetone. (g) Remove the residual PDMS thin film to complete the removal of a hybrid stamp. (h) The stacking process is repeated to complete the fabrication process,

which includes bonding with a hard substrate.

## 2.4. Results and Discussion

The purpose to utilize a hybrid stamp in the molding process is to remove the protruding edges of the molded PDMS structures. If the stamp is made purely of PDMS, the contact surface is relatively soft. When a pressure is applied on a stamp to clear PDMS residuals at through-layer regions, the stamp at contact regions deforms. Since uncured PDMS is solidified between a deformed stamp and a mold, protruding edges are formed and transferred to the molded structures. These non-flat surfaces inhibit follow-up bonding with other structures. This problem becomes severe when small features are transferred since the protruded edges can occupy a significant area on these features. Tight contact required for good bonding between layers is not allowed. A similar deformation issue also occurs in the alternative approach of creating through-layer PDMS structures using a soft master mold and a hard stamp. In the case of a hard master mold and a hard stamp combination, the uncured PDMS residuals at the through-layer regions cannot be completely removed. The novelty of the plastic embedded hybrid stamp is to provide a stiff stamp to prevent deformation, while keeping a required elasticity at the contact interface to ensure a complete removal of uncured PDMS at through-layer regions. The plastic plate has a Young's module of $E$=3.2GPa, much larger than the

PDMS Young's modulus(E=0.6MPa). Figure 2-2(a,b) and (c,d) shows the degree of edge deformation of PDMS structures molded by a standard PDMS stamp and a hybrid stamp, respectively. In Figure 2-2(d), an open microfluidic channel with HAR (5:1) PDMS walls is demonstrated. Figure 2-3 shows a multilayer PDMS structure with pneumatically driven microvalves sandwiched between two hard, transparent, and electrically conductive ITO glass substrates. In addition, a 30 μm thick PDMS membrane with a high-density array of HAR through-layer vias that are 6 μm in diameter has also been successfully fabricated, as shown in Figure 2-4. The pitch between vias is 100 μm. Table 1 summarizes recent representative works on fabrication of 3D microfluidics structure. Parameters including lateral resolution, layer thickness resolution, hard substrate bonding ability, and HAR value are provided for comparison with the current work. The resolution and HAR value of our current approach is limited by the resolution of photolithography for making the master mold. To create a HAR structure with a lateral resolution of 6 μm, the maximum thickness we can achieve is 30 μm due to the optical diffraction limit when patterning a thick photoresist.

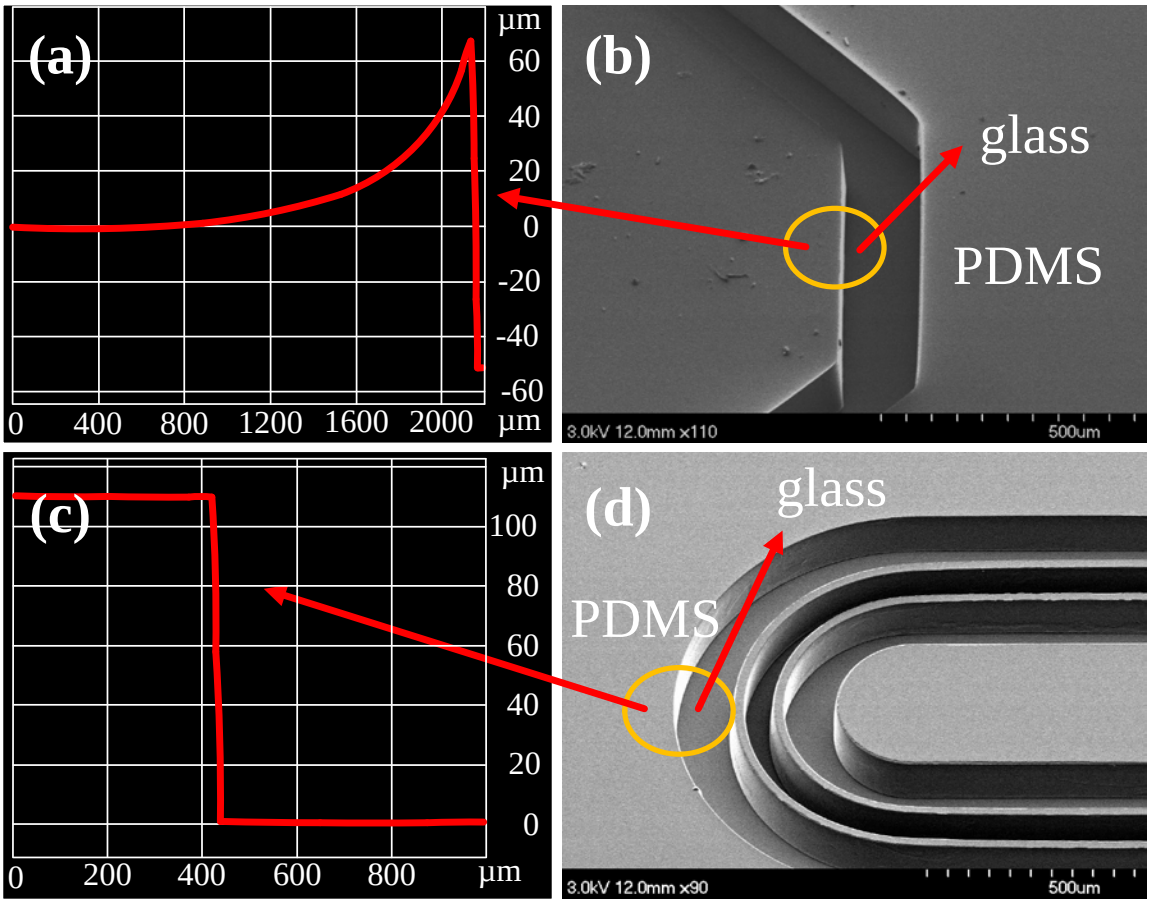


Figure 2-2 (a, b) Edge protrusion issue near open structures of a PDMS thin film fabricated with a standard elastic PDMS stamp. This issue can be eliminated by using a plastic sheet embedded hybrid stamp in the molding process as shown in (c, d). Without the embedded plastic sheet, the contact surface is soft and results in protrusion edge around the channel. With the hybrid stamp, the contact surface is much more rigid to prevent the edge protrusion, and retains its ability to handle freestanding HAR sidewall structure.

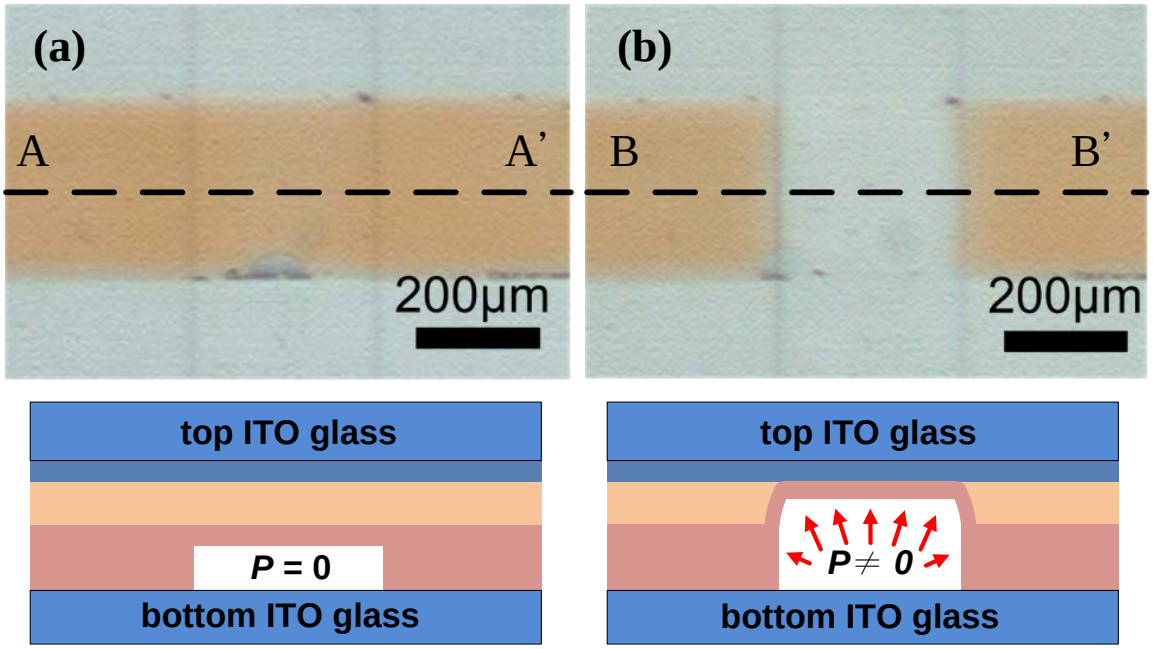


Figure 2-3 Two layers of thin film PDMS structure with integrated pneumatic microvalve are bonded and sandwiched between two ITO coated glass substrates. (a) The top layer with fluidic channel is filled with dye liquid. The bottom layer is filled with uncolored DI water. The pneumatic pressure applied to the bottom channel P=0, which causes no valve membrane deformation. The subset shows the cross-sectional view along AA' line. (b) When a sufficient pneumatic pressure P is applied to the bottom channel, the valve membrane deforms and fully closed the top channel. The subset shows the cross-sectional view along BB' line.

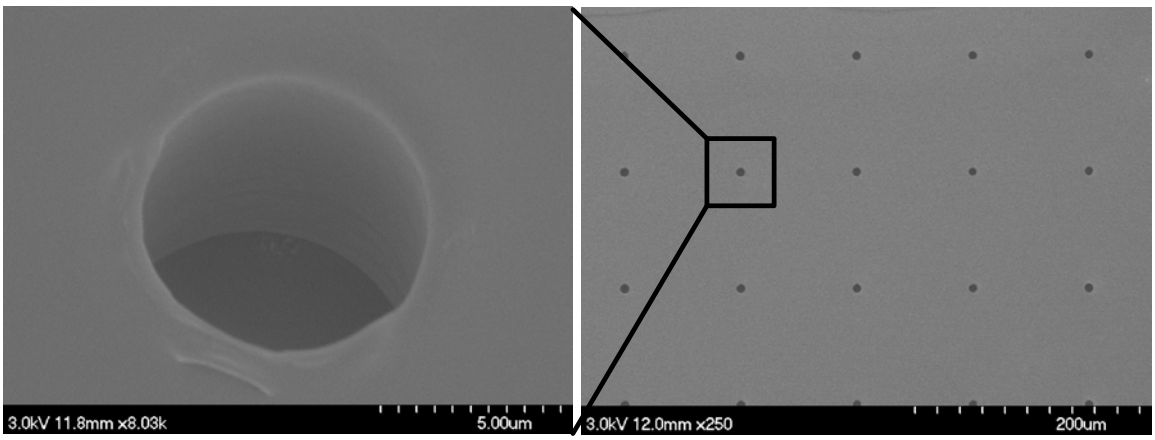


Figure 2-4 SEM images of a 30 µm thick PDMS membrane with an array of 6 µm wide through-layer holes.

## 2.5. High Aspect Ratio Deformable Membranes for 3D DEP Focusing

In addition to providing three-dimensional fluid routing, the ability to fabricate vertical, thin, HAR PDMS membranes and bond them with hard substrates allows the fabrication of deformable channels. This unique advantage promises novel functional devices not possible before, especially in fields such as electrokinetics, optofluidics, and inertial microfluidics, in which the channel cross-section profile plays a critical role in underlying device physics. For example, particle focusing equilibrium locations can change in a high-speed inertia flow when the channel deforms; and a curved and deformed channel can work as a tunable lens for light focusing and collection in optofluidics.

Here, we demonstrate a novel electrokinetics device that can achieve tunable 3D cell focusing in the center of a channel without sheath flows. Figure 2-5(a,b) shows the schematic of such a device fabricated using the hybrid stamp approach. A single layer PDMS thin film with high aspect ratio (HAR=4) walls is bonded between two

featureless ITO glass substrates. Figure 2-5(c) shows the picture of a completed microfluidic device. By applying pressure to the two side channels, the middle channels can be deformed as shown in Figure 2-5 (b). Application of an electrical bias to the two featureless ITO electrodes causes electric field streamlines to be focused in the middle neck of the deformed channel, creating a highly non-uniform electric field distribution with the maximum field enhancement occurring in the center. (Figure 2-5(d)).

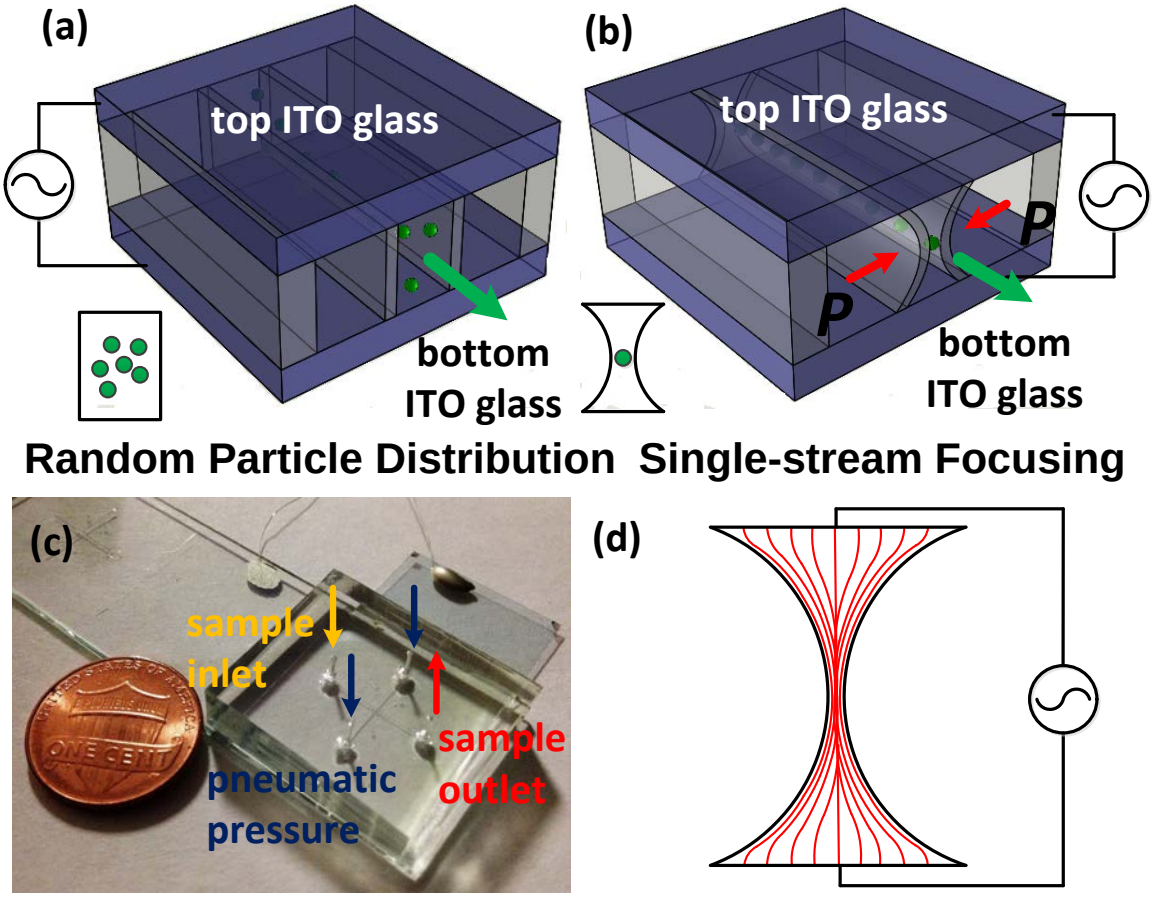


Figure 2-5 Schematic of a tunable 3D DEP focusing device. (a) An open PDMS microchannel with thin, high-aspect-ratio sidewalls is sandwiched between two conductive indium tin oxide (ITO) coated glass substrates. An a.c. signal is applied between the top and bottom substrate. (b) When the channel sidewalls are pressurized, the channel deforms to form a narrow neck in the middle and focus the electric field

lines. Positive DEP responding particles would migrate to the center of the channel where the maximum electric field occurs. (c) Photograph of a fabricated device. (d) A schematic showing crowding electric field streamlines in the neck of a deformed channel.

Figure 2-6(a), (b) show the microscope images of a channel with vertical sidewalls of 80 µm high and 20 µm thick before and after a pressure of 60psi is applied to the side channels, respectively. An alternating current (a.c.) signal is applied to the top and bottom ITO electrode to provide the electric field required for cell focusing using dielectrophoresis.

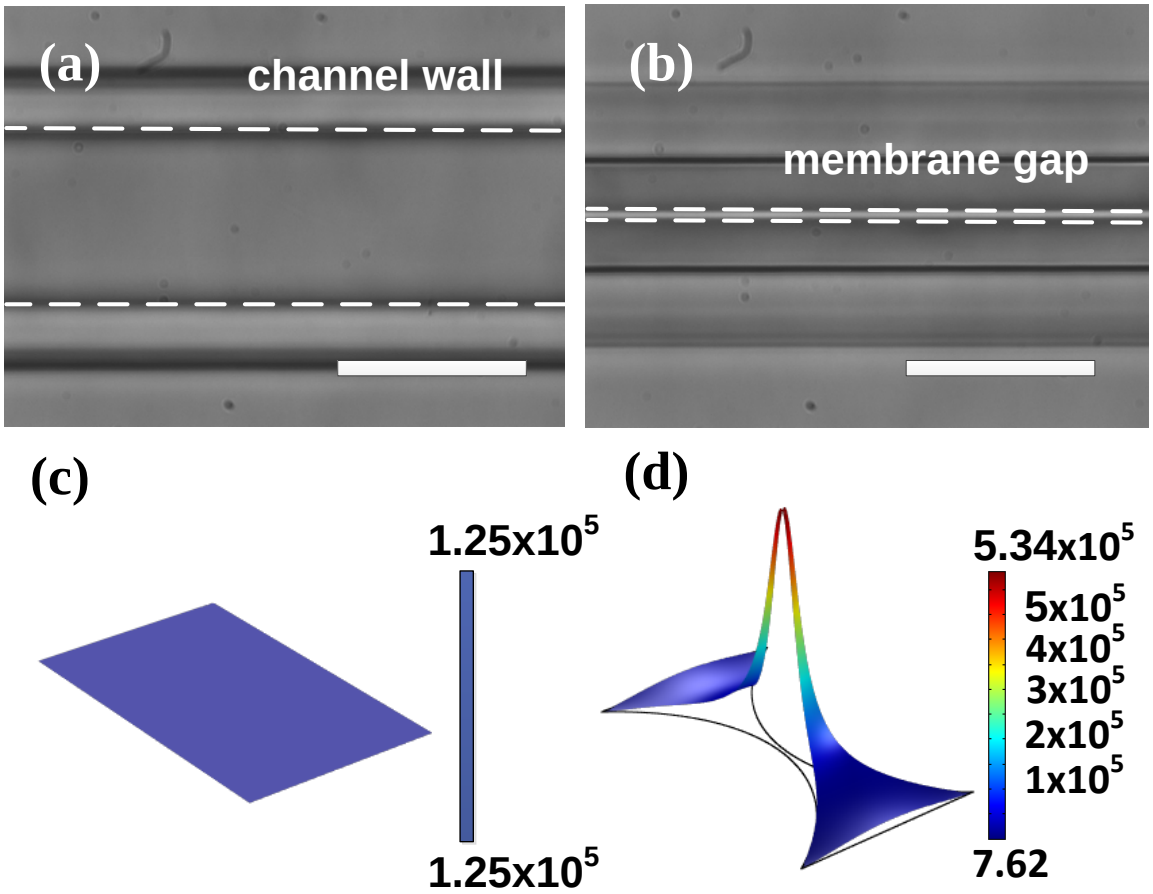


Figure 2-6 (a) Microscopy images of a deformable microchannel with a dimension of 50µm in width, 80µm in height, and a sidewall thickness

of 20 µm. (b) The channel sidewalls are under of pressure of 60psi. (c) Electric field distribution in a microchannel without deformation under an ac bias of 10V peak-to-peak at a frequency of 5MHz. (d) When the channel is deformed to form a neck that is only 0.5µm width, strong field enhancement is generated in the middle of this channel. Scale bar : 50µm

Dielectrophoresis (DEP) is a phenomenon in which a particle in a non-uniform electric field can experience an electrostatic force moving the particle towards stronger electric field regions if the particle is more polarizable than the medium, called positive DEP. A particle moves to weaker electric field regions if the particle is less polarizable than the medium, called negative DEP [28] [29] [30-33]. To migrate a particle in an electric field using dielectrophoresis, there must be electric field gradient. In a uniform electric field region, although particles are polarized, no net DEP forces can be induced for moving.

Figure 2-6(c)(d) compares the simulated electric field distribution in a channel with and without deformation, respectively. Since the sidewalls can be continuously deformed to eventually contact each other and seal the gap, this device allows the tuning of the electric field strength in the middle of the channel by controlling the applied pressure in the side channels. The narrower the neck, the larger the electric field enhancement is generated in the neck. This allows the creation of strong electric field gradients for focusing small objects such as bacteria. Cells or particles experiencing positive DEP forces in the channel are attracted to the center of the channel, providing a continuous 3D sheathless cell focusing function for potential applications in microfluidic flow cytometers and cell sorters.

The performance of 3D DEP focusing on this deformable channel is tested using two types of cells, GFP-Hela with a diameter of 15µm and GFP-E. Coli with rod shape of 2 µm long and 700 nm in diameter. Before pumping the sample into the device, GFP-Hela cells was suspended in an isotonic buff0er consisting of 8.5% sucrose and 0.3% dextrose and with a conductivity of 10mS/m. GFP-E. Coli was suspended in a buffer solution of 10% sucrose in 20 mM HEPES and with a conductivity of 30mS/m. The sample was injected continuously into the microchannel by a syringe pump (kdScientific, 780100). A function generator (Agilent, 33220A) and power amplifier (ENI, Model 2100L) were used to provide the a.c. voltage source. The DEP response of the cells were monitored under an inverted fluorescence microscope (Carl Zeiss, Axio Observer.A1), and recorded by a CCD camera (Carl Zeiss, AxioCam MRm). For the HeLa-GFP focusing, the side channel was pressured at 35psi to create a 16µm wide gap, roughly the size of HeLa cells. When an a.c. signal (300kHz, 56.6V peak-to-peak) was applied, GFP-Hela cells were focused to the center of the channel (Figure 2-7(b)), and remained focused in the downstream even at regions without deformed channels due to the laminar flow nature in microfluidics. To focus E. Coli, the sidewalls of the channel is further deformed to a smaller gap of only 3 µm to create a stronger electric field strength and gradient for focusing these smaller objects. When there was no a.c. signal applied, GFP-E. Coli were randomly distributed across the channel (Figure 2-7(c)). Under the application of an a.c. signal (5MHz, 56.6V peak-to-peak), positive DEP forces focused GFP-E. Coli to the center of the channel to form a single stream fluorescence trace as shown in Figure 2-7(d).

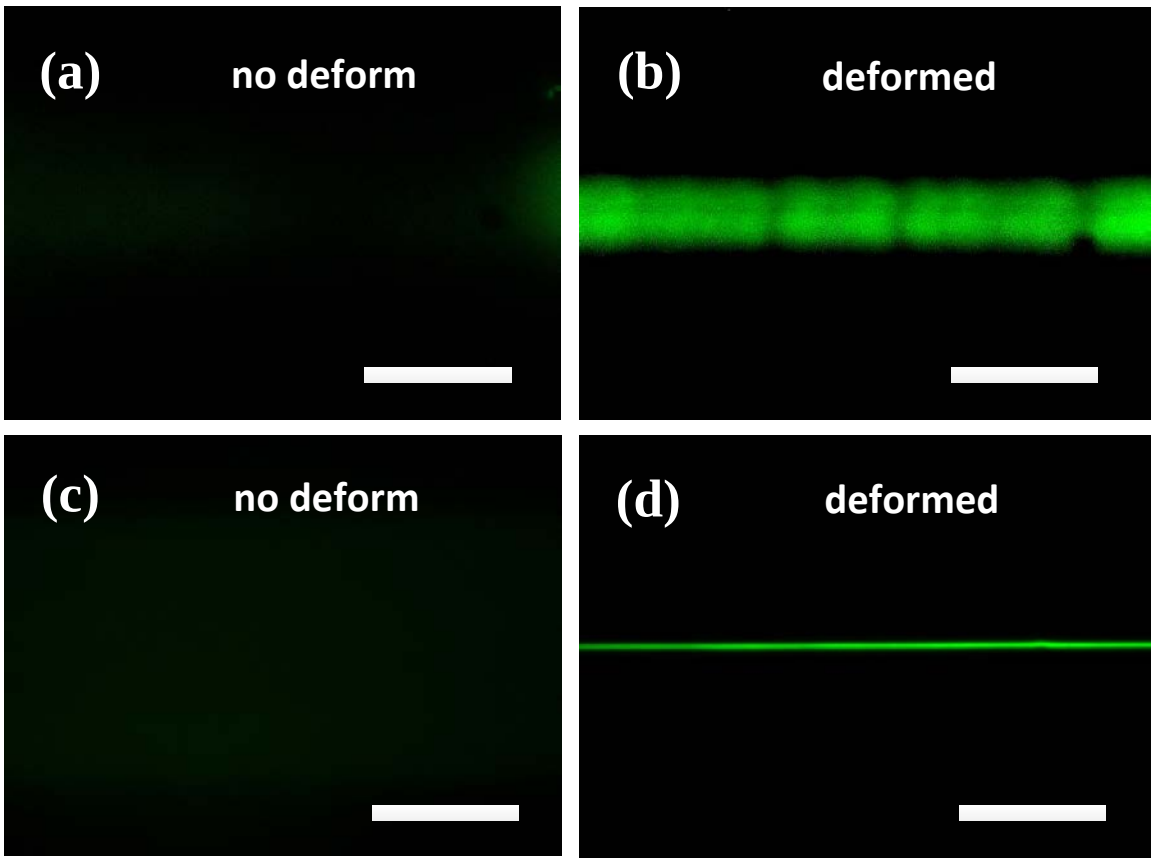


Figure 2-7 The focused fluorescence traces of biological objects. All samples are suspended in media with conductivities ranging from 10 mS/m to 30 mS/m. An a.c. signal of 56.6V peak-to-peak with frequencies varying from 300 kHz to 5 MHz is applied. (a, b) compare the fluorescence traces of GFP-Hela (spherical shape, 15µm in diameter) in a channel without and with sidewall deformation (35 psi) at an average flow speed of 17 cm/sec. The channel neck in (b) is 16 µm; (c, d) compare the traces of GFP-E. coli (rod-shape, 2µm long and 700nm wide) in a channel without and with sidewall deformation (60 psi) deformation at an average flow speed of 14 cm/sec. The channel neck in (d) is 3 µm. Scale bar : 25µm

## 2.6. Conclusion

This chapter demonstrates a new fabrication approach capable of manufacturing multilayer, 3D, HAR, open PDMS based microfluidic structures that can be bonded between hard substrates. This approach utilizes a hybrid stamp that consists of a plastic plate embedded right underneath a thin PDMS film to provide the required hardness for preventing severe stamp deformation during molding processes. A thin layer of PDMS film on the plastic plate provides local elasticity to ensure a complete removal of uncured residual PDMS in the through-layer regions. HAR PDMS structures fabricated by this method do not have protruding edges and offer flat interfaces for multilayer stacking and bonding with hard substrates. Using this unique fabrication capability, we demonstrate deformable channel formed by sandwiching thin, vertical, HAR PDMS channel walls between two ITO substrates. These thin channel sidewalls can be continuously deformed under pressure to change the cross-section of a channel, a feature that may find many applications in fields such as optofluidics, inertial microfluidics, and electrokinetics that have channel profile sensitive physical phenomena. To demonstrate, we utilized this deformable channel structure to achieve single stream, 3D, sheathless focusing of mammalian cells as well as small bacteria.

## 2.7. Reference

1. Yeo, L.Y., et al., Microfluidic Devices for Bioapplications. Small, 2011. 7(1): p. 12 - 48.

2. J. Shi, S.Y., S.-C. Steven Lin, X. Ding, I.-K. Chiang, K. Sharp, Tony J. Huang, Three-dimensional continuous particle focusing in a microfluidic

channel via standing surface acoustic waves (SSAW). Lab on a Chip, 2011. 11: p. 2319-2324.

3. J. Shi, X.M., D. Ahmed, A. Colletti, Tony J. Huang, Focusing microparticles in a microfluidic channel with standing surface acoustic waves (SSAW). Lab on a Chip, 2008. 8: p. 221 - 223.

4. Y. Chen, A.A.N., Y. Zhao, P.-H. Huang, J. Phillip McCoy, Stewart J. Levine, L. Wang, Tony J. Huang, Standing surface acoustic wave (SSAW)-based microfluifdic cytometer. Lab on a Chip, 2014. 14: p. 916-923.

5. Chen, Y., et al., 3D pulsed laser-triggered high-speed microfluidic fluorescence-activated cell sorter. Analyst, 2013. 138: p. 7308-7315.

6. Fan, Y.J., et al., Three dimensional microfluidics with embedded microball lenses for parallel and high throughput multicolor fluorescence detection. BIOMICROFLUIDICS, 2013. 7(4): p. 044121.

7. Huh, D., et al., Reconstituting Organ-Level Lung Functions on a Chip. Science, 2010. 328(No. 5986): p. 1662 - 1668.

8. Jang, Y.-H., et al., An integrated microfluidic device for two-dimensional combinatorial dilution. Lab on a Chip, 2011. 11(19): p. 3277 - 3286.

9. Kim, J., et al., A programmable microfluidic cell array for combinatorial drug screening. Lab on a Chip, 2012. 12(10): p. 1813 - 1822.

10. Liu, M.C., D. Ho, and Y.-C. Tai, Monolithic fabrication of three-dimensional microfluidic networks for constructing cell culture array with an integrated combinatorial mixer. Sensors and Actuators B: Chemical, 2008. 129(2): p. 826 - 833.

11. Liu, M.C. and Y.-C. Tai, A 3-D microfluidic combinatorial cell array. Biomedical Microdevices, 2011. 13(1): p. 191 - 201.

12. Ostuni, E., et al., Patterning Mammalian Cells Using Elastomeric Membranes. Langmuir, 2000. 16(20): p. 7811 - 7819.

13. Wang, Y., et al., Capture and 3D culture of colonic crypts and colonoids in a microarray platform. Lab on a Chip, 2013. 13(23): p. 4625-4634.

14. Gregory, C.W., et al., High yield fabrication of multilayer polydimethylsiloxane devices with freestanding micropillar arrays. BIOMICROFLUIDICS, 2013. 7(5): p. 0565503.

15. Brassard, D., et al., 3D thermoplastic elastomer microfluidic devices for biological probe immobilization. Lab on a Chip, 2011. 11(23): p. 4099-4107.

16. Agirregabiria, M., et al., Fabrication of SU-8 multilayer microstructures based on successive CMOS compatible adhesive bonding and releasing steps. Lab on a Chip, 2005. 5: p. 545 - 552.

17. Patel, J.N., et al., SU-8- and PDMS-based hybrid fabrication technology for combination of permanently bonded flexible and rigid features on a single device. JOURNAL OF MICROMECHANICS AND MICROENGINEERING, 2013. 23(6): p. 065029.

18. Patel, J.N., et al., PDMS as a sacrificial substrate for SU-8-based biomedical and microfluidic applications. JOURNAL OF MICROMECHANICS AND MICROENGINEERING, 2008. 18: p. 095028.

19. Unger, M.A., et al., Monolithic Microfabricated Valves and Pumps by Multilayer Soft Lithography. Science, 2000. 288(5463): p. 113 - 116.

20. Hong, J.W. and S.R. Quake, Integrated nanoliter systems. Nature Biotechnology, 2003. 21: p. 1179 - 1183.

21. Thorsen, T., S.J. Maerkl, and S.R. Quake, Microfluidic Large-Scale Integration. Science, 2002. 298(5593): p. 580-584.

22. Kartalov, E.P., et al., Microfluidic vias enable nested bioarrays and autoregulatory devices in Newtonian fluids. Proceedings of the National Academy of Sciences of the United States of America, 2006. 103(33): p. 12280–12284.

23. Kang, J.H., E. Um, and J.-K. Park, Fabrication of a poly(dimethylsiloxane) membrane with well-defined through-holes for three-dimensional microfluidic networks. JOURNAL OF MICROMECHANICS AND MICROENGINEERING, 2009. 19: p. 045027.

24. Zhang, M., et al., A simple method for fabricating multi-layer PDMS structures for 3D microfluidic chips. Lab on a Chip, 2010. 10(9): p. 1199 - 1203.

25. Carlborg, C.F., et al., A High-Yield Process for 3-D Large-Scale Integrated Microfluidic Networks in PDMS. JOURNAL OF MICROELECTROMECHANICAL SYSTEMS, 2010. 19(5): p. 1050 - 1057.

26. Karlsson, J.M., et al., Fabrication and transfer of fragile 3D PDMS microstructures. JOURNAL OF MICROMECHANICS AND MICROENGINEERING, 2012. 22(8).

27. Li, M., et al., A simple and cost-effective method for fabrication of integrated electronic-microfluidic devices using a laser-patterned PDMS layer. Microfluidics and Nanofluidics, 2012. 12(5): p. 751-760.

28. Khoshmanesh, K., et al., Dielectrophoretic Platforms for Bio-microfluidic Systems. Biosensors and Bioelectronics, 2011. 26(5): p. 1800-1814.

29. Pethig, R., Review Article—Dielectrophoresis: Status of the theory, technology, and applications. BIOMICROFLUIDICS, 2010. 4(2): p. 022811.

30. Barbulovic-Nad, I., et al., DC-dielectrophoretic separation of microparticles using an oil droplet obstacle. Lab on a Chip, 2006. 6(2): p. 274-279.

31. Cummings, E.B. and A.K. Singh, Dielectrophoresis in Microchips Containing Arrays of Insulating Posts : Theoretical and Experimental Results. Analytical Chemistry, 2003. 75(18): p. 4724-4731.

32. Kang, K.H., et al., Continuous separation of microparticles by size with Direct current-dielectrophoresis. Electrophoresis, 2006. 27(3): p. 694-702.

33. Salmanzadeh, A., et al., Isolation of prostate tumor initiating cells (TICs) through their dielectrophoretic signature. Lab on a Chip, 2011. 12(1): p. 182-189.

# CHAPTER 3

## TUNNEL DIELECTROPHORESIS FOR TUNABLE, SINGLE-STREAM CELL FOCUSING IN HIGH SPEED MICROFLUIDIC FLOWS IN PHYSIOLOGICAL BUFFERS

### 3.1. Abstract

Three-dimensional (3D) single-stream cell or microparticle focusing in confined channels is a critical function in high throughput biological analysis. Current methods of microparticle and cell focusing are limited because of sample dilution, spatial resolution, and controllability issues. Herein, we demonstrate a novel dielectrophoresis (DEP) mechanism for tunable, sheathless, three dimensional, and single-stream microparticle and cell focusing in high-speed flows. It is realized by fabricating a 3D microfluidic device, which can provide DEP forces completely perpendicular to the hydrodynamic flows along the entire several centimeter-long channel. This new approach provides, for the first time, real-time three dimensional tuning of focusing locations by simply changing voltage combinations applied to electrodes. In addition, microparticle and mammalian cell focusing is achieved in high-speed flow in regular physiological buffers, without medium swapping to low ionic isotonic buffers as in most prior DEP based devices.

## 3.2. Introduction

Particles in different streamlines in a microfluidic channel flow at different speeds due to the parabolic flow velocity distribution resulting from the zero-slip boundary conditions and viscous fluid environment. Focusing randomly distributed particles into a narrow stream in a continuous flow allows all particles to flow at the same speed and in the same cross-section location. This function is critical for applications that need accurate synchronization and coordination of particles in both space and time domains. For example, flow cytometer one of the most efficient and effective approaches for single cell analysis. One of the core features of a flow cytometer is the ability to three-dimensionally focus cells and particles into a single stream. This allows all particles and cells travelling at an identical speed through an optical detection zone such that all particles receive the same illumination intensity and time for reliable and consistent optical detection [1]. Fluorescence activated cell sorter (FACS) is a special type of flow cytometer that adds a downstream sorting function to select target particles detected in the upstream. Tight particle focusing is extremely important to synchronize the detection and switching event. Without particle focusing, particle flow speed varies and the arrival time of particles into the switching zone is difficult to predict, which results in failure of sorting out target particles or cells. For many other particle

sorting techniques that are based on magnetic forces, dielectrophoresis, acoustics, inertial forces, tight particle focusing is also important to provide particles and cells of different properties a common reference in space for high efficiency and high purity sorting.

Particle focusing can be achieved by many prior approaches. Traditionally, sheath fluid is used to sandwich the sample fluid in a co-flow manner. The laminar flow nature in microfluidics allows tight focusing to be achieved by using a large sheath-to-sample fluid ratio. However, serious dilution of sample is a potential concern for many applications. Tuning particle focusing location can be realized by changing the input sheath flows, yet it takes some time before the new equilibrium focusing location becomes stabilized. To eliminate the need of sheath flows for focusing, some other approaches have been developed.

Inertia effects of particles flowing in high-speed flows have recently been found significant in microfluidic channels. Particles can be focused to into few equilibrium streams where hydrodynamic forces on particles resulting from flow velocity gradient and wall effects are equal. Single stream microparticle focusing can also be achieved by using secondary flows induced by periodic structures[2-5]. Some limitations of inertial focusing include size-dependent focusing location, insensitive to small sized particles, and the need of high-speed flows. Tuning

focusing stream location in real-time might be challenge since the equilibrium positions are dependent upon channel geometry and flow speed.

Acoustic focusing is another broadly applied mechanism. By forming standing acoustic waves in microfluidic channels, either through bulk acoustic waves (BAW) [6-10] or surface acoustic waves (SAW) [8-10], particles and cells can be focused to nodal points. Acoustic focusing approaches can provide tunable focusing functions by either adding an additional echo channel in the BAW cases[11, 12] or using chirped inter-digital transducers (IDT) as in the SAW-based approaches[13, 14]. However, such tuning is currently limited to one dimension across the channel, and multiple focusing positions across the channel cross section.

Dielectrophoretic forces have also been utilized to provide focusing functions in microfluidics. This electrical based mechanism provides a great tuning flexibility since the applied voltages can be continuously and easily adjusted in real-time. However, limited DEP forces, typically in the orders of tens of pN, prevent most current DEP devices from providing tight focusing functions in high-speed flows[15-17], which also limit their throughputs. Furthermore, DEP devices usually require the manipulated particles and cells to be suspended in isotonic buffers with low ionic strength to increase DEP forces and responsibility of cells.

Such low ionic buffers, different from regular physiological buffers, may impact cells' physiological conditions and viability.

Here, we demonstrate a novel tunnel dielectrophoresis (TDEP) mechanism for tunable, sheathless, three dimensional, and single-stream microparticle and cell focusing in high-speed flows. It is realized by fabricating a 3D microfluidic device with two glass substrates sandwiching a thin and open PDMS channel (see supplementary materials for detailed fabrication process). Electrodes are laid out to provide DEP forces completely perpendicular to the hydrodynamic flow along a channel of several centimeter-long. This provides a long DEP interaction such that microparticles and cells have sufficient time to migrate to the focused stream even in high-speed flows. Figure 3-1 shows the schematic of a TDEP device. Four independently tunable a.c. signals are applied to these quadro-electrodes to create a tunnel-shape potential energy landscape with a cross-sectional single minimum in the center of a channel along the channel. The location of the potential minimum, as well as the particle and cell focusing location, can be real-time tuned in two dimensions across the cross section by changing the voltage combinations applied to these electrodes. Of note is that, due to the completely perpendicular and decoupled design between the DEP and hydrodynamic forces, the focusing location is flow speed independent. The focused location is also particle type independent as

along as they show negative DEP responses to the applied electrical signals. In addition, microparticles and mammalian cells focusing can be achieved in physiological buffers without medium swapping to low ionic buffers prior to DEP operations.

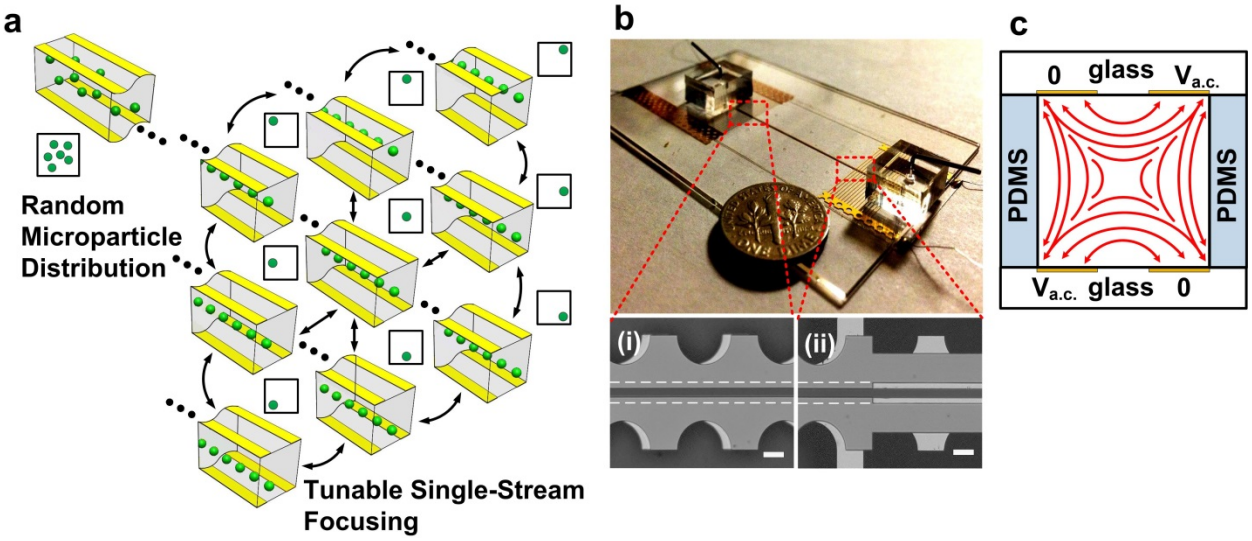


Figure 3-1. Schematic design concept and example device of FD-DEP for tunable 3D particle focusing. (a) The quadro-electrodes are longitudinally aligned with the microchannel. Different a.c. signals are applied symmetrically or asymmetrically to the four corner electrodes. Randomly distributed particles can be focused into single-stream in the downstream at different cross-section locations where a.c. electric field minima are located. (b) A 6cm-long-channel FD-DEP device with an U.S. 1 dime coin for scale, (b-i) and (b-ii) show the corresponding microscope images of the device in the inlet and outlet. (c) Cross section view of the device. A PDMS thin film with an open trench of

80µm x 83µm (W X H) microchannel is sandwiched between two glass substrates with quadro-electrodes aligned along the

### 3.3. Device Design and Operation Principle

Dielectrophoresis refers to the interaction force between a non-uniform electric field and the dipole moment it induces on a polarizable object. The magnitude of DEP force on a spherical particle can be expressed by the following formula derived based on a diploe approximation.

$$F_{DEP}^{(1)} = 2\pi\varepsilon_m R^3 \,\mathrm{Re}\left[ CM\left(\omega\right)\times\nabla\overline{E}^2 \right] \tag{1}$$

where $F_{DEP}^{(1)}$ refers to the DEP force, $\varepsilon_m$ the permittivity of the medium surrounding the sphere, *R* the radius of the particle, ω the radian frequency of the applied field, and $\overline{E}$ the applied electric field. *CM* is the Clausius-Mossotti (CM) factor given by

$$CM = \frac{\underline{\varepsilon}_p - \underline{\varepsilon}_m}{\underline{\varepsilon}_p + 2\underline{\varepsilon}_m} \tag{2}$$

Where $\underline{\varepsilon}_p$ and $\underline{\varepsilon}_m$ are the complex permittivities of the particle and the medium, respectively, and $\underline{\varepsilon} = \varepsilon + \sigma/(j\omega)$, where $\varepsilon$ is the permittivity, $\sigma$ the conductivity. The magnitude of DEP force is linearly proportional to the gradient of electric field strength ($E^2$) and the volume of particles. For particles more polarizable than the medium, Re [CM]>0, they experience positive DEP forces that move them toward the strong

electric field region. On the other hand, if Re[CM]<0, particles migrate to the weak electric field region.

DEP manipulation on mammalian cells is usually conducted in low ionic isotonic buffers for several reasons. One is that different types of mammalian cells suspended in low ionic buffers (0.01 S/m ~ 0.1 S/m) can show very distinct dielectric signatures and CM curves, which makes cell sorting easier to perform. Second, higher voltage can be applied to electrodes to generate larger DEP forces on cells without inducing electrolysis on electrodes or causing significant heating. Yet, suspending cells in isotonic buffers with low ionic strength over a long time may impact cells' viability.

The challenge of manipulating mammalian cells in regular physiological buffers is that only negative DEP forces can be induced on cells since the Re[CM] is negative and small over the entire frequency spectrum. In addition, high frequency, typically 1 MHz to 10 MHz, and low voltage operation is required to prevent electrolysis on electrodes. This limits the DEP forces that can be induced on mammalian cells in physiological buffers. The design of TDEP has several unique features to solve these challenges. TDEP is for focusing particles and cells with negative DEP forces. The four independently voltage controlled quadro-electrodes ensure that there is only one potential minimum in the cross section of a microfluidic channel. The location of potential minimum

can be real-time tuned by changing the voltage combinations applied to electrodes. In TDEP, there is only one focused position for all particles, regardless of their sizes and types, as long as they show negative DEP responses. This is an important feature for applications, such as flow cytometers, that need all particles to flow at the same speed, pass through the same location in a channel for light detection or imaging, and be at the same reference position for downstream applications. The extremely long DEP interaction distance throughout the entire channel allows cells in physiological buffers with weak negative DEP forces to have sufficient time to migrate to the focused location in high-speed flows. For example, if the DEP induced cell migration speed is 80 um/sec, and the channel width and height are both 80 um. It takes an average of 0.5 second for cells near the channel wall to migrate to the center of the channel. If the DEP interaction distance is 6 cm, the length used in TDEP devices presented in this paper, single stream focusing can be realized at an average flow speed of 12 cm/sec, two orders of magnitude higher than prior DEP focusing devices that operate at a flow speed < 1 mm/sec. [33] Long DEP channel can be easily fabricated by utilizing a serpentine channel design. However, running cells at a speed higher than 10 cm/sec in a microfluidic channel may encounter inertial effects that affect the DEP focusing functions. More studies are

required to understand the coupling between inertial forces and DEP forces in this regime.

Another unique feature of TDEP is that the DEP forces on cells and particles only exist in the direction perpendicular to the channel and completely decouple from the hydrodynamic forces that carry particles to flow along a streamline in the channel. This means that particles' transverse migration driven by DEP forces is not affected by the flow speeds in channels. Unlike prior DEP devices that utilized titled electrode design for cell focusing, DEP forces and hydrodynamic forces are not decoupled. Particle focusing behavior is highly dependent upon flow speeds, particle sizes, and particle types. [34-37]

## 3.4. Results and Discussion

### 3.4.1. Fabrication Method

**Step 1**: Fabrication of master molds.

It starts from fabricating SU-8 mold masters on silicon wafers using photolithography (Figure 3-2(a)). SU8 3050 negative photoresist is used as a mold with the height of 83μm. The mold needs to be surface treated with trichloro (1H,1H,2H,2H-perfluorooctyl) silane (97%, Sigma-Aldrich, USA), also called PFOCTS, to facilitate later demolding. This surface treatment was carried out in a vacuum chamber at a pressure of -30 psi for 16 hours.

**Step 2**: Fabrication of hybrid stamps.

It starts from preparing the Sylgard 184 silicone elastomer mixture (Dow Corning Corporation, Miland, USA). The ratio of Base : Curing agent is 10g : 1g. Few drops of this mixture are poured into a petri dish. A suitable size of polystyrene plastic plate is cut and pressed against the bottom of the petri dish under a pressure of 3 psi. A thin layer of polydimethylsiloxane (PDMS) with a thickness of roughly 30μm is formed between the petri dish and the plastic plate. Additional uncured PDMS is poured to fill up the petri dish, followed by a curing step at 600C in an oven for 12 hours. A hybrid stamp is formed when the plastic plate together with a thin PDMS layer on its surface is peeled off from the petri dish (Figure 3-2(b)). The hybrid stamp is also surface treated with PFOCTS as in Step 1 for 6 hours. To fabricate PDMS thin film with through-layer structures, uncured PDMS is poured onto the master mold, pressed by the hybrid stamp under a pressure of 4psi, and cured at 500C in an oven for an hour.

**Step 3**: Demolding PDMS films from master mold.

During the demolding process, the cured PDMS thin film has stronger adhesion to the hybrid stamp than to the master mold since more PFOCTS is coated on the master mold due to a longer treatment time (Figure 3-2(c)).

**Step 4**: Transfer and stack PDMS thin films.

Oxygen plasma treatment is performed on both the PDMS thin film on the hybrid stamp and the bottom substrate to be bonded for two minutes. In this case, both top and bottom substrates are glass slides and coverslips with strip electrodes patterned by lift-off process. Large area alignment between hybrid stamp and bottom substrate are performed under a microscope before bonding (Figure 3-2(d)). The bonded set is baked in an oven at $60^0$C for 2 hours.

**Step 5**: Removing hybrid stamp.

It starts from peeling off the bulk PDMS part on the plastic plate (Figure 3-2(e)), followed by dissolving the polystyrene plastic plate in an acetone bath for 4 hours (Figure 3-2(f)). This leaves a thin residual PDMS film on the substrate that can be easily peeled off from the device due to prior PFOCTS treatment (Figure 3-2(g)) to finish the transferring process of a PDMS thin film with through-layer structures. This mechanically gentle releasing technique allows us to transfer PDMS thin film to fragile substrates, such as a glass cover slip, over a large area.

**Step 6**: Top cover substrate assembly

Finally, the device is aligned with top substrate without oxygen plasma bonding. Gentle attachment is performed to sealed the device. (Figure 3-2(h)).

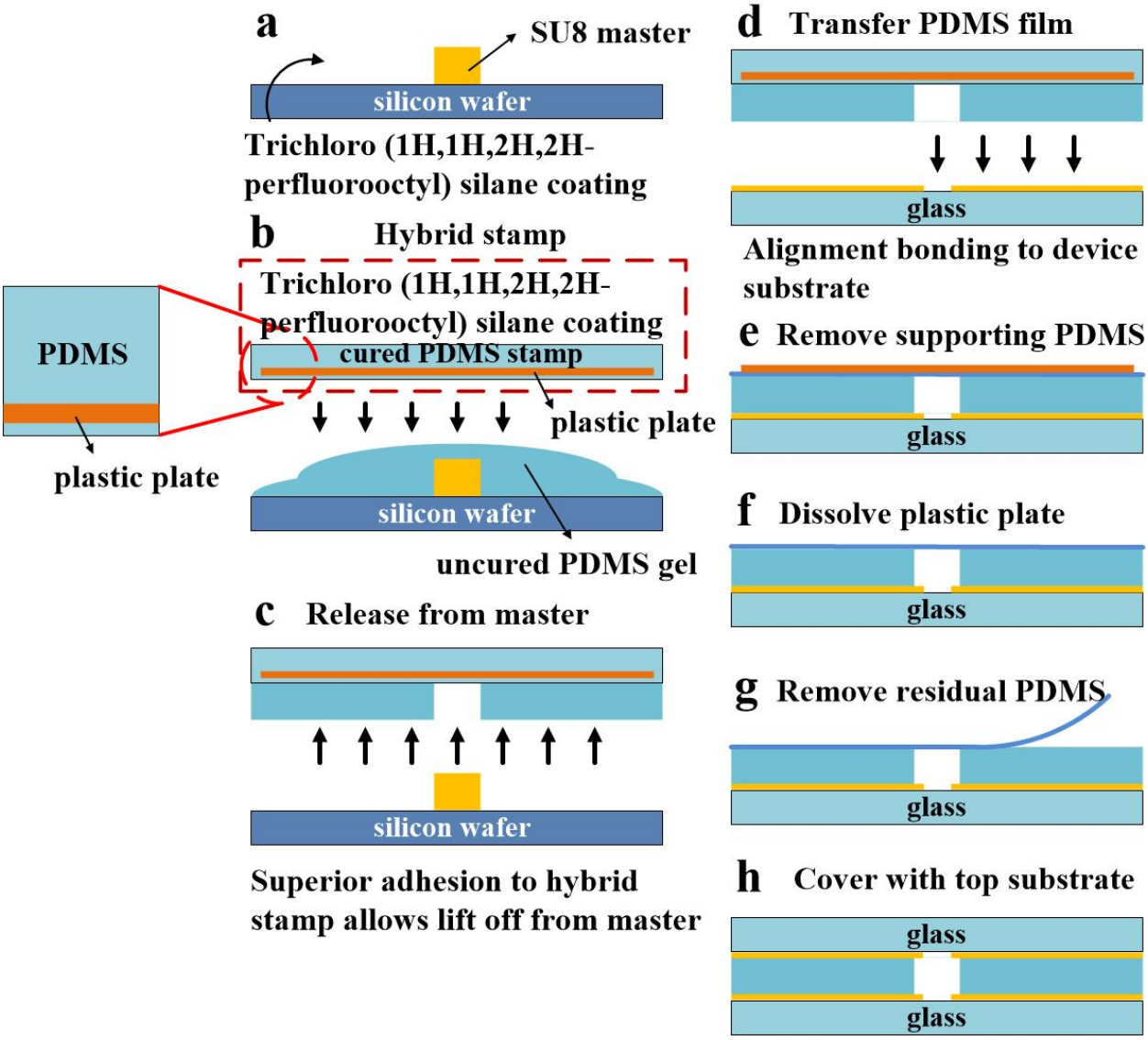


Figure 3-2 Schematic of fabrication process flow using a plastic plate embedded hybrid stamp. (a) A SU8 3050 master is treated with PFOCTS to facilitate later demolding. (b) Uncured PDMS mixture is poured on

the master, and pressed against the hybrid stamp. (c) Due to less PFOCTS treatment on the hybrid stamp compared to the master, the casted PDMS film tends to adhere to the hybrid stamp and allows to be peeled off from the master. (d) The film is aligned and bonded by oxygen plasma treatment (e) Remove the support PDMS on the hybrid stamp. (f) Dissolve the polystyrene plastic plate in acetone. (g) Remove the residual PDMS thin film to complete the removal of a hybrid stamp. (h) The device and top substrate are aligned and sealed without oxygen plasma bonding.

### 3.4.2. 3D Tunable Focusing

The four independently controlled quadro-electrodes provide the real-time tuning function to adjust the location of potential minimum and particle focused stream. Figure 3-3(a) shows the COMSOL numerical simulation results of electric field distribution across a rectangular channel under different voltage combinations. When symmetric voltage signals are applied (Figure 3-3(a-v)), the electric field minimum is located at the center of the channel. When one of the voltages is changed to ΔV or V-ΔV, where ΔV < V, the focusing position will shift in one of the diagonal directions as shown in Figure 3-3(a-i,iii,vii,ix). For lateral or vertical shifts, two of the voltages are changed to ΔV and V-ΔV. Depending on which two electrodes are picked, lateral shifts are shown in Figure 3-3(a-iv, vi), and vertical shifts in Figure 3-3(a-

ii,viii). The amount of shift depends on the amplitude of ΔV and can be continuously tuned. The tuning range, in principle, can be as large as the entire channel cross section. For example, if the ΔV in Figure 3-3(a-iii) is equal to V, the electric field minimum will be at the upper right corner of the channel. In real applications, shifting particles too close to walls may not be preferred since particle speed will be significantly slowed down due to the parabolic flow velocity profile in a microfluidic channel.

These simulation results are confirmed by experimental data shown in Figure 3-3(b) that shows the stacked confocal images of polystyrene beads flowing through a rectangular TDEP channel under the application of different voltage combinations. The experiment was conducted using a 6 cm long TDEP channel. The confocal images were taken at 4 cm in the downstream channel location where beads were already tightly focused into a single stream. The TDEP channel is 80 μm wide and 83 μm high; the average flow speed is 5 cm/sec; the maximum a.c. voltage applied is 10Vp-p at 1MHz frequency; and the solution was a PBS buffer with a conductivity of 1 S/m. These experimental results not only prove that particle focusing in TDEP is electrically tunable but also show that there is only one electric field

minimum across the channel for single stream focusing in all cases shown.

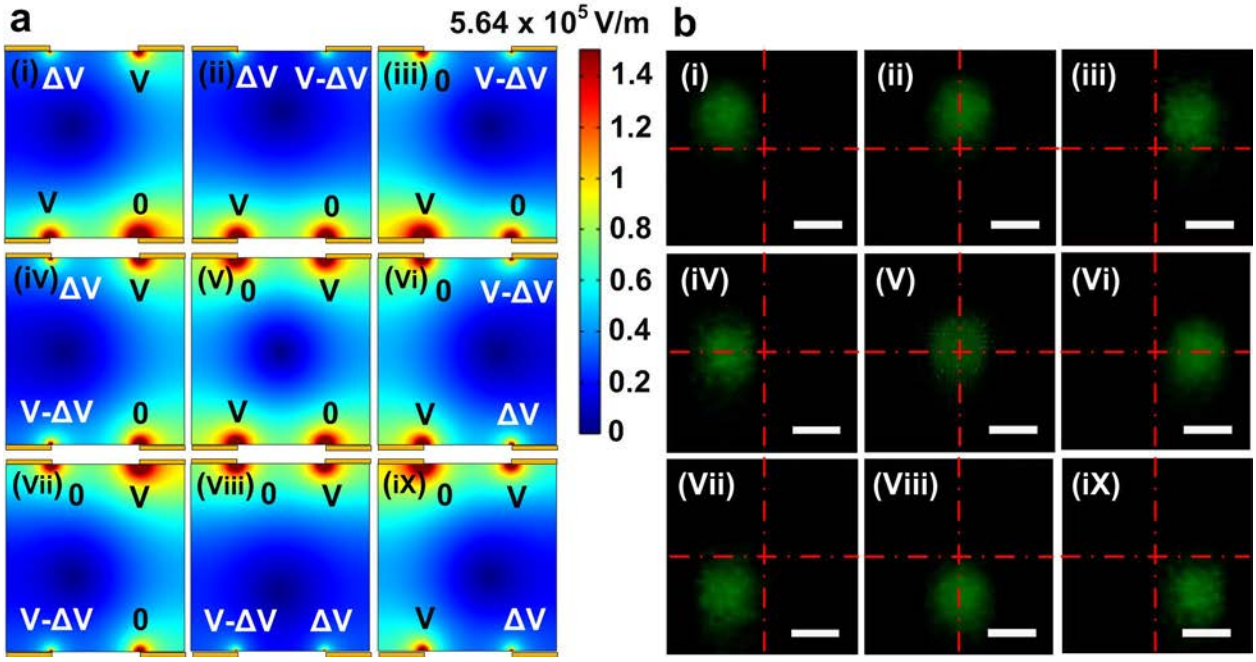


Figure 3-3 Electric field simulation and confocal cross-section images of focused particle stream. (a) Electric field simulation on the cross-section of a 80µm x 83µm (W x H) microchannel used for DEP focusing. As shown in (a-v), when symmetric voltages (V, 0, V, 0) are applied to the quadro-electrodes, electric field minimum is located right at the center of the channel. As a differential voltage of either ΔV or V-ΔV replaces one of the applied voltages in (a-v), the electric field minimum would be offset diagonally as shown in (a-i) upper-left shift, (a-iii) upper-right shift, (a-vii) bottom-left shift, and (a-ix) bottom-right shift. When differential voltages, ΔV and V-ΔV replace two of the applied voltages in

(a-v), the electric field minimum would offset laterally as shown in (a-iv) left shift, (a-vi) right shift, and vertically as shown in (a-ii) top shift, (a-viii) bottom shift. The amount of offset can be continuously tuned by adjusting the amplitude of ΔV. In this simulation, liquid medium is assumed having conductivity of 1 S/m with V = 10Vp-p and ΔV = 3.1Vp-p under 1MHz of excitation frequency. (b) Stacked confocal images showing the focused 10μm polystyrene particles in the downstream where particles are tightly focused at different cross-sectional locations. Particles focusing positions can be continuously tuned laterally (iv,vi), vertically (ii,viii), or diagonally (i,iii,viii,ix) or any other arbitrary locations in the cross section through different combinations of voltages. Images were taken under an average flow speed of 5cm/s with a maximum 10Vp-p, 1MHz, a.c. signals. Scale bar : 10μm

### 3.4.3. Size Independent Focusing

In Figure 3-4, we demonstrated the function of size-independent particle focusing. The focusing positions of microparticles can be precisely predicted by COMSOL numerical simulation (Figure 3-4(a-c)) and verified experimentally by the high-speed microscopic images shown in Figure 3-4(d-f) demonstrating that different sizes of particles (9μm, 15μm, 20μm) are all focused tightly into a single stream with submicron position variations in all cases (Figure 3-4(d-f)). Standard

variations of ±0.46μm, ±0.33μm, and ±0.39μm were found for the cases of 14 μm shift toward the left, zero shift, and 14 μm shift to the right, respectively (Figure 3-4(g-i)).

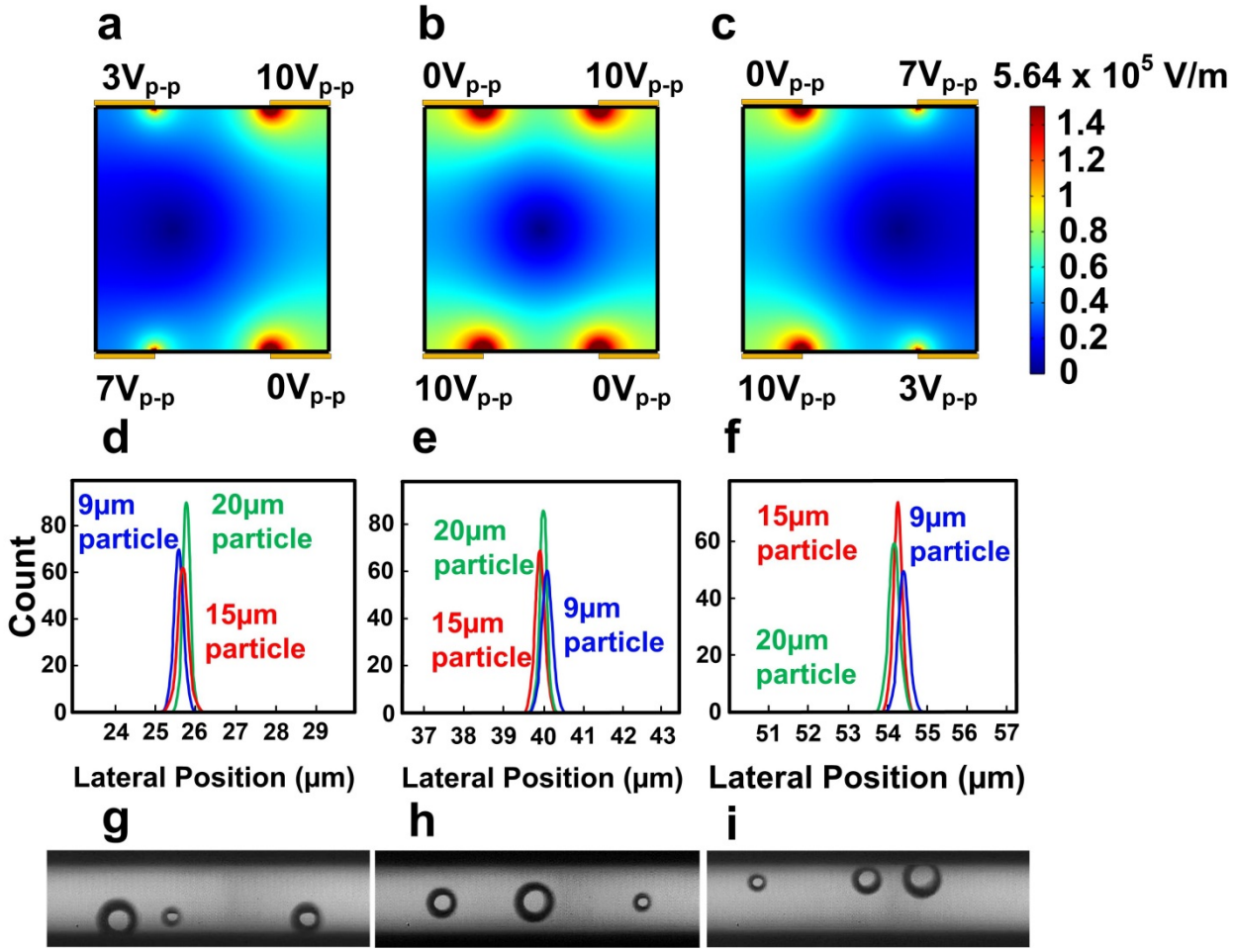


Figure 3-4 Size independent focusing experiment. (a-c) Numerical simulation of electric field distribution for three different focusing locations in the TDEP channel under the application of three different sets of voltages. (d-f) High-speed microscopic images showing four different sizes of polystyrene beads (9μm, 15μm, 20μm) are all focused into a single stream in all cases. (g-i) Size independent and tight

focusing is proved by the small standard deviations of ±0.46μm, ±0.33μm, and ±0.39μm, respectively. The average flow speed used for this study is 5cm/s.

### 3.4.4. Mammalian Cell Focusing and Viability Study

The snapshot images in Figure 3-5(a-c) captured by the high-speed camera show the lateral tunable focusing of THP1 cells in a physiological buffer (PBS, conductivity ~1S/m). A 13.8Vp-p, 10MHz symmetric a.c. signal is applied in Figure 3-5(b) to focus cells flowing at a speed of 11cm/s. Because of the size- and type-independent focusing nature of the TDEP platform, different sizes of cells can be well focused as shown in the histogram Figure 3-5(e), in which the standard deviation falls within 0.82μm. For non-symmetric voltage excitation, an a.c. signal sets with a maximum 15.4Vp-p, 10MHz are applied to focus THP1 cells flowing at a speed of 8.7cm/s into a stream with a 12.5 um lateral offset as shown in Figure 3-4(a,c). Figure 3-4(d) and Figure 3-4(f) show the focusing histogram of Figure 3-5(a) and Figure 3-5(c) with variations of 0.76μm and 0.89μm, respectively.

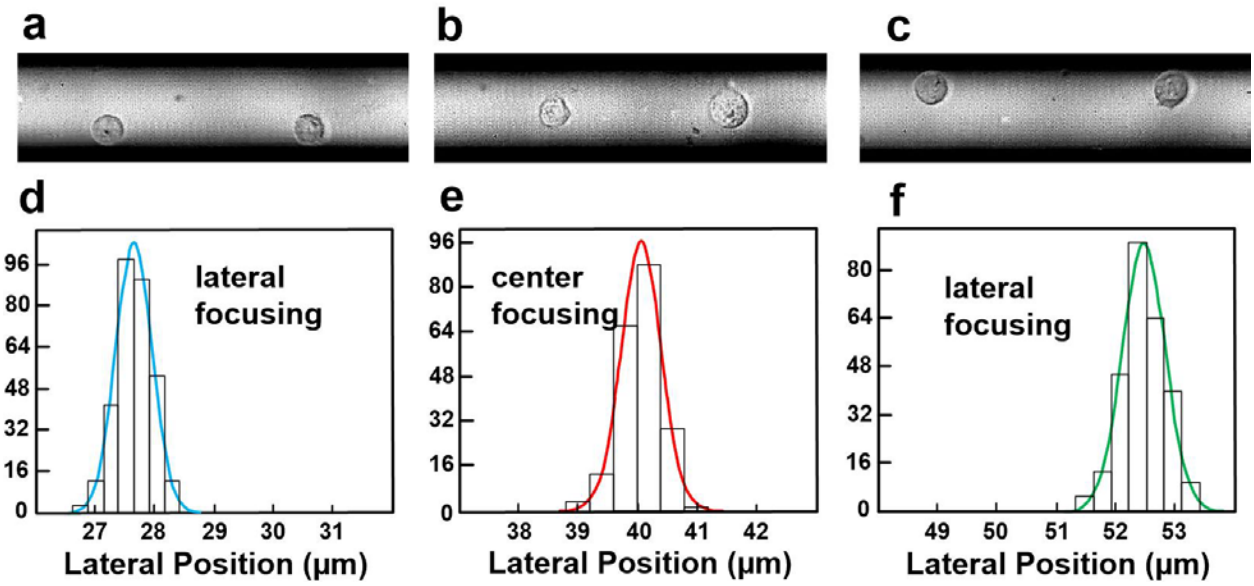


Figure 3-5 High-speed images showing lateral tunable focusing of THP1 cells. (a) THP1 cells were biased as the case shown in Fig. 2(a-iv). A maximum voltage of 15.4Vp-p, 10MHz is applied to focus cells flowing at a speed of 8.7cm/s with a 12.5 μm offset from the center. (b) Symmetric a.c. voltages (13.8 Vp-p, 10MHz ) are applied as in the case of Fig. 2(a-v) to focus cells flowing at a speed of 11cm/s in the center of a channel. (c) Voltages in (a) are reversely applied to shift the focusing stream to the other side. (d-f) Focusing histograms showing the lateral distribution of cells for (a-c). The spatial variations are 0.76μm, 0.82μm, 0.89μm, respectively.

In order to verify the viability effect before and after DEP focusing operation, short-term and long-term viability tests were carried out. In the short-term viability test, THP1 cells in condition of Fig. 4(b) were collected after the experiments and compared with cells without focusing operation as shown in Fig. 5(d). Experiment was carried out continuously for one hours. Right after the experiment, cells were stained with Propidium iodide (PI) and verified the viability by flow cytometer. Cells before DEP operation has an average viability of 92.6%, and cells right after DEP operation has an average viability of 87.2%, which shows no major short-term viability issue. As for the long-term viability test, HeLa cells were used for the DEP operation. Under the same experimental condition of Fig. 5(b) for one hour, HeLa cells right after the focusing experiment were put back into cell culture medium DMEM (Dulbecco's Modified Eagle Medium) inside incubator for long-term culturing. Fig. 6 (a-c) shows microscopy images of HeLa cells captured after DEP focusing and cultured at day 0, day 2, and day 4, respectively. From which, HeLa cells can proliferate normally without seeing any viability issues.

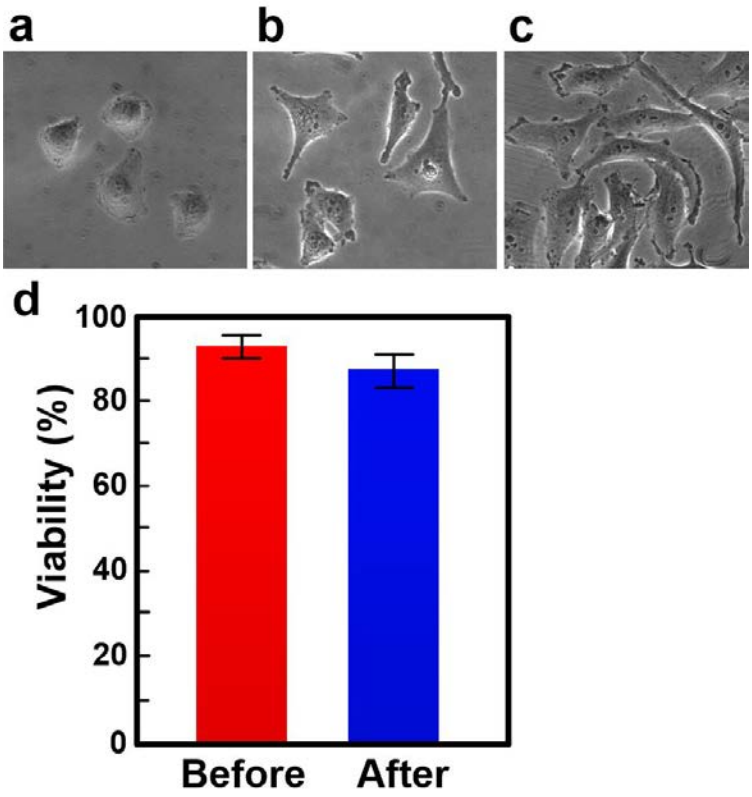


Figure 3-6 Viability tests before and after DEP focusing operation. A 13.8Vp-p, 10MHz symmetric a.c. signal is applied (Fig. 3-2(a(v)) in to focus HeLa cells continuously for one hours for long-term and short-term viability tests. (a-c) HeLa cells were collected after the experiment, and put back into cell culture medium DMEM (Dulbecco's Modified Eagle Medium) inside incubator for long-term culturing. Microscopy images of HeLa cells were captured after DEP focusing and cultured at day 0, day 2, and day 4, respectively. From which, HeLa cells can proliferate normally without seeing any viability issues. (d) HeLa cells were collected after the experiment, and stained with Propidium iodide (PI) and verified the viability by flow cytometer. Cells before DEP

operation has an average viability of 92.6%, and cells right after DEP operation has an average viability of 87.2%, which shows no major short-term viability issue.

### 3.5. Reference

1. Cram, L.S., Flow cytometry, an overview. Methods in Cell Science, 2002. 24(1): p. 1-9.

2. Chen, Y., et al., Pulsed Laser Activated Cell Sorting with Three Dimensional Sheathless Inertial Focusing. Small, 2014. 10(9): p. 1746-1751.

3. Chung, A.J., D.R. Gossett, and D.D. Carlo, Three dimensional, sheathless, and high-throughput microparticle inertial focusing through geometry-induced secondary flows. Small, 2013. 9(5): p. 685-690.

4. Chung, A.J., et al., Microstructure-induced helical vortices allow single-stream and long-term inertial focusing. Lab on a Chip, 2014. 13(15): p. 2942-2949.

5. Lee, M.G., S. Choi, and J.-K. Park, Three-dimensional hydrodynamic focusing with a single sheath flow in a single-layer microfluidic device. Lab on a Chip, 2009. 9(21): p. 3155-3160.

6. Antfolk, M., et al., Focusing of sub-micrometer particles and bacteria enabled by two-dimensional acoustophoresis. Lab on a Chip, 2014. 14(15): p. 2791-2799.

7. Grenvall, C., et al., Two-dimensional acoustic particle focusing enables sheathless chip Coulter counter with planar electrode configuration. Lab on a Chip, 2014. 14(24): p. 4629-4637.

8. Chen, Y., et al., Standing surface acoustic wave (SSAW)-based microfluidic cytometer. Lab on a Chip, 2014. 14(5): p. 916-923.

9. Shi, J., et al., Focusing microparticles in a microfluidic channel with standing surface acoustic waves (SSAW). Lab on a Chip, 2008. 8(2): p. 221-223.

10. Shi, J., et al., Three-dimensional continuous particle focusing in a microfluidic channel via standing surface acoustic waves (SSAW). Lab on a Chip, 2011. 11(14): p. 2319-2324.

11. E. J. Fong, A.C.J., T. Notton, S.-Y. Jung, K. A. Rose, L. S. Weinberger, M. Shusteff, Acoustic focusing with engineered node locations for high-performance microfluidic particle separation. Analyst, 2014. 139(5): p. 1192-1200.

12. Jung, S.-Y., et al., Spatial tuning of acoustofluidic pressure nodes by altering net sonic velocity enables high-throughput, efficient cell sorting. Lab on a Chip, 2015. 15(4): p. 1000-1003.

13. Ding, X., et al., Standing surface acoustic wave (SSAW) based multichannel cell sorting. Lab on a Chip, 2012. 12(21): p. 4228-4231.

14. Li, S., et al., An On-Chip, Multichannel Droplet Sorter Using Standing Surface Acoustic Waves. Analytical Chemistry, 2013. 85(11): p. 5468-5474.

15. Haandbæk, N., et al., Resonance-enhanced microfluidic impedance cytometer for detection of single bacteria. Lab on a Chip, 2014. 14(17): p. 3313-3324.

16. Holmes, D., H. Morgan, and N.G. Green, High throughput particle analysis: Combining dielectrophoretic particle focussing with confocal optical detection. Biosensors and Bioelectronics, 2006. 21(8): p. 1621-1630.

17. Morgan, H., D. Holmes, and N.G. Green, 3D focusing of nanoparticles in microfluidic channels. IEEE Proc.-Nanobiotechnol, 2003. 150(2): p. 76 - 81.

18. Gao, J., et al., Electrokinetic focusing and separation of mammalian cells in conductive biological fluids. Analyst, 2012. 137(22): p. 5215-5221.

19. Han, K.-H. and A.B. Frazierb, Lateral-driven continuous dielectrophoretic microseparators for blood cells suspended in a highly conductive medium. Lab on a Chip, 2008. 8(7): p. 1079-1086.

20. Hu, X., et al., Marker-specific sorting of rare cells using dielectrophoresis. Preceedings of the National Academy of Sciences of the United States of America, 2005. 102(44): p. 15757-15761.

21. Kim, U., et al., Multitarget Dielectrophoresis Activated Cell Sorter. Analytical Chemistry, 2008. 80(22): p. 8656-8661.

22. Kim, U., et al., Selection of mammalian cells based on their cell-cycle phase using dielectrophoresis. Preceedings of the National Academy of Sciences of the United States of America, 2007. 104(52): p. 20708-20712.

# CHAPTER 4

## TUNABLE, HIGH-SPEED, AND 3D MICROFLUIDIC DEVICE FOR ULTRA-HIGH PRECISION SIZE-BASED PARTICLE SEPARATION

### 4.1. Abstract

Following up the tunable ultra-high precision particle focusing in chapter 3, in this chapter, I utilized the true advantages of TDEP and immediate novel and important application on ultra-high precision microparticle and cell focusing and separation in high-speed flows. For the first time, particle size difference as small as 1μm can be separated with high purity (>90%). This is realized by a 3D tunable, size-independent, single-stream sub-micron precision (variation <0.2 μm) focusing function. Tunable electric field patterns are enabled by simply changing voltage combinations applied to electrodes. Microparticle and mammalian cell focusing and separation is achieved at flow speeds up to 3 cm/s in high conductivity regular physiological buffers.

### 4.2. Introduction

Accurate and high throughput cell sorting technologies are critical for applications in molecular and cellular biology, biotechnology, and medicine [1]. Biological, chemical, or medical processes involving complex fluids with embedded particles (e.g., blood) often require preparative separation of particles, cells, or even molecules that are

needed for subsequent procedures. In conventional macroscale separation processes, centrifugation and membrane filtration approaches have been commonly used for decades, whereas more sophisticated methods such as fluorescence-activated cell sorting (FACS) and magnetically activated cell separation (MACS) were rapidly established as the standard methods for high quality cell and particle separation. While conventional methods can provide highly efficient label-based sorting in short timescales, advances in microfluidics have enabled miniature devices not only offering similar capabilities [2-7], but also unprecedented label-free sorting functions by exploiting a variety of physical parameters as biomarkers, such as cell size, deformability, compressibility, shape, density, size, surface properties, electrical polarizability, magnetic susceptibility and refractive index. Among these, cell size is the most straight-forward feature and sorting based on size can be easily accessible through microfiltration [8], pinched flow fractionation [9], inertial microfluidics[10], acoustophoresis[11], and dielectrophoresis [12]. However, a high throughput and reliable approach is still lacking for high purity sorting of particles with small size difference.

To achieve continuous and high size precision sorting two stages of particle manipulation methodologies are required. In the first stage, all particles, regardless of their different sizes, have to be three-

dimensionally focused into a single-stream in a continuous flow such that different sizes of particles have exactly the same reference position. In the second stage, particles migrate to a new focusing position under a new set of boundary conditions. Due to different forces acting on particles of different sizes, particles of different migration speeds can be sorted out and collected. A size-independent, tight upstream particle focusing is the key for the downstream high purity sorting of particles with minor size differences.

Here, I demonstrate a novel DEP device that can provide a microfluidic device capable of providing tunable and particle size-independent, sub-micron precision single-stream focusing in the upstream [13], and followed by high purity sorting of particles with size difference smaller than 1μm in the downstream. Furthermore, such sorting was achieved at flow speeds up to 3 cm/s in regular physiological buffers, without the need to swap the medium to a low ionic isotonic buffer, which may affect cells' viability and physiological conditions.

### 4.3. Device Design

Dielectrophoresis (DEP) is a phenomenon in which a particle in a non-uniform electric field can experience an electrostatic force moving it towards a stronger electric field region if it is more polarizable than the medium, or to a weaker electric field region if the particle is less

polarizable than the medium. To migrate a particle in an electric field using dielectrophoresis, there must be electric field gradient. Otherwise, in a uniform electric field region, although particles are polarized, no net DEP forces can be induced to move particles.

Figure 4-1 shows the schematic of a 3D microfluidic device capable of performing tunable, sheathless, three dimensional, and single-stream microparticle and cell focusing in high-speed flows. It is realized by sandwiching a thin and open PDMS channel between two glass substrates. Electrodes are laid out to provide DEP forces completely perpendicular to hydrodynamic flows along the entire channel [13, 14]. The principle of tunable electric field pattern is achieved by applying different combinations of ac voltages to four corner electrodes to offset the electric field potential minima in the channel cross section. In the upstream focusing section (Figure 4-1(ii)), particles of different sizes are all focused to a single-stream to one side of the channel. In the downstream separation section (Figure 4-1(iii)), focusing spot is programmed to offset to the other side. Larger particles drift faster laterally than smaller ones and migrate into the collection channel. Confocal fluorescence images show the cross-sectional particle position in the upstream (Figure 4-1(ii)) and downstream sections (Figure 4-1(iii)).

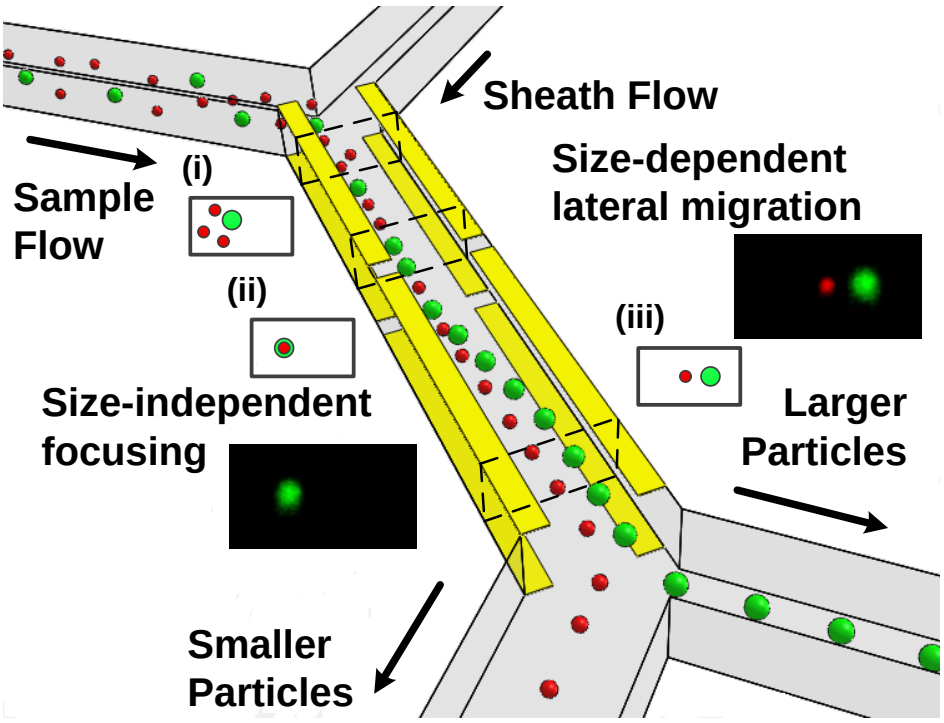


Figure 4-1 Schematic of the DEP based device for ultra-high precision particle focusing and sorting. Two pairs of quadro-electrodes are longitudinally aligned with the microchannel. Different a.c. signals are applied asymmetrically to the four corner electrodes. Randomly distributed particles of different sizes can be focused into a single stream in the upstream and laterally migrate to new focusing location in the downstream. Larger particles drift faster than the small ones, and get collected into the collection channel.

## 4.4. Results and Discussion

### 4.4.1. Fabrication Method

**Step 1**: Fabrication of master molds.

It starts from fabricating SU-8 mold masters on silicon wafers using photolithography (Figure 4-2(a)). SU8 3050 negative photoresist is used as a mold with the height of 83µm. The mold needs to be surface treated with trichloro (1H,1H,2H,2H-perfluorooctyl) silane (97%, Sigma-Aldrich, USA), also called PFOCTS, to facilitate later demolding. This surface treatment was carried out in a vacuum chamber at a pressure of -30 psi for 16 hours.

**Step 2**: Fabrication of hybrid stamps.

It starts from preparing the Sylgard 184 silicone elastomer mixture (Dow Corning Corporation, Miland, USA). The ratio of Base : Curing agent is 10g : 1g. Few drops of this mixture are poured into a petri dish. A suitable size of polystyrene plastic plate is cut and pressed against the bottom of the petri dish under a pressure of 3 psi. A thin layer of polydimethylsiloxane (PDMS) with a thickness of roughly 30µm is formed between the petri dish and the plastic plate. Additional uncured PDMS is poured to fill up the petri dish, followed by a curing step at 600C in an oven for 12 hours. A hybrid stamp is formed when the plastic plate together with a thin PDMS layer on its surface is peeled off from the petri dish (Figure 4-2(b)). The hybrid stamp is also surface treated with PFOCTS as in Step 1 for 6 hours. To fabricate PDMS thin film with through-layer structures, uncured PDMS is poured onto the

master mold, pressed by the hybrid stamp under a pressure of 4psi, and cured at 500C in an oven for an hour.

**Step 3**: Demolding PDMS films from master mold.

During the demolding process, the cured PDMS thin film has stronger adhesion to the hybrid stamp than to the master mold since more PFOCTS is coated on the master mold due to a longer treatment time (Figure 4-2(c)).

**Step 4**: Transfer and stack PDMS thin films.

Oxygen plasma treatment is performed on both the PDMS thin film on the hybrid stamp and the bottom substrate to be bonded for two minutes. In this case, both top and bottom substrates are glass slides and coverslips with strip electrodes patterned by lift-off process. Large area alignment between hybrid stamp and bottom substrate are performed under a microscope before bonding (Figure 4-2(d)). The bonded set is baked in an oven at $60^0$C for 2 hours.

**Step 5**: Removing hybrid stamp.

It starts from peeling off the bulk PDMS part on the plastic plate (Figure 4-2(e)), followed by dissolving the polystyrene plastic plate in an acetone bath for 4 hours (Figure 4-2(f)). This leaves a thin residual PDMS film on the substrate that can be easily peeled off from the

device due to prior PFOCTS treatment (Figure 4-2(g)) to finish the transferring process of a PDMS thin film with through-layer structures. This mechanically gentle releasing technique allows us to transfer PDMS thin film to fragile substrates, such as a glass cover slip, over a large area.

**Step 6**: Top cover substrate assembly

Finally, the device is aligned with top substrate without oxygen plasma bonding. Gentle attachment is performed to sealed the device. (Figure 4-2(h)).

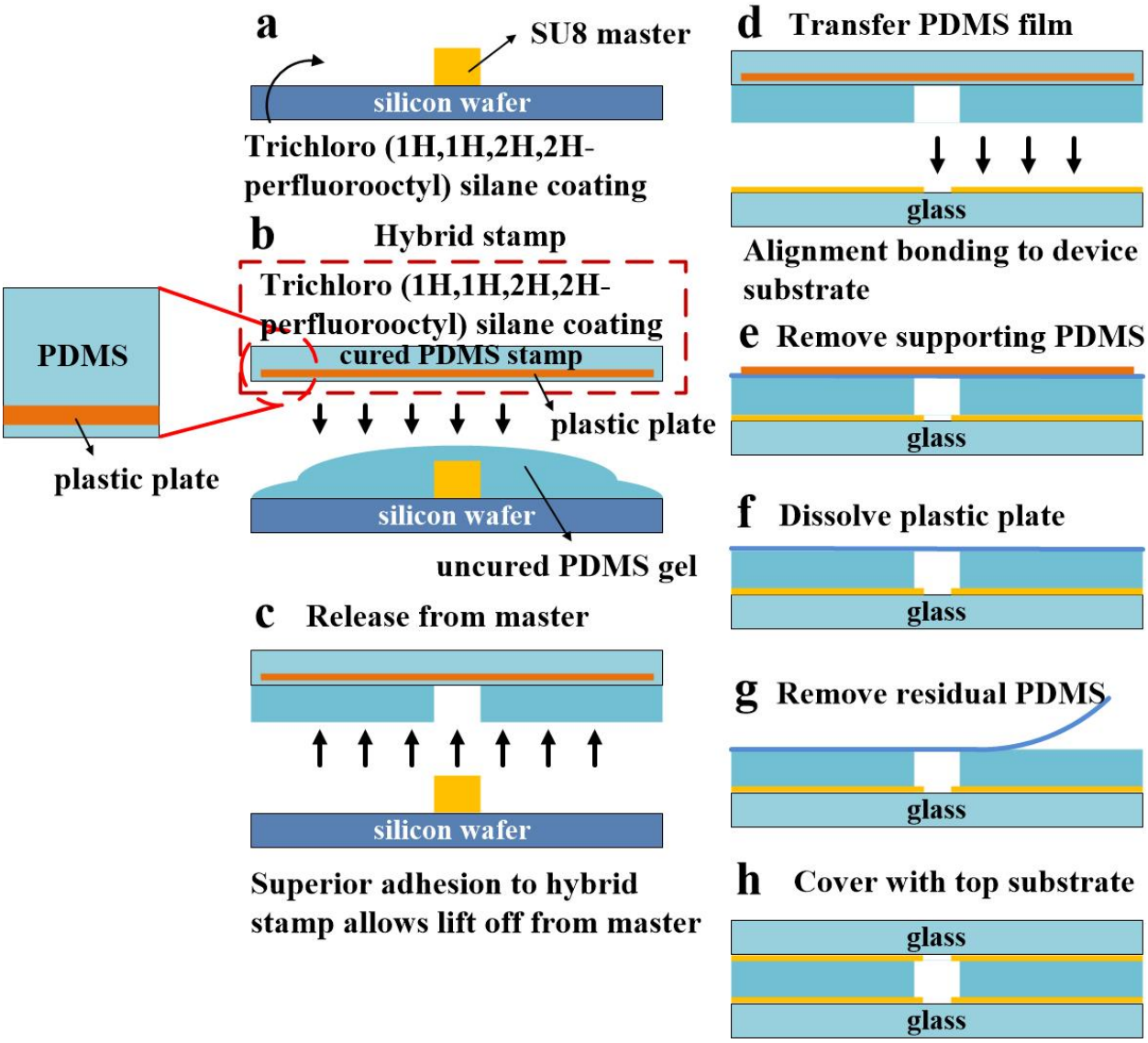


Figure 4-2 Schematic of fabrication process flow using a plastic plate embedded hybrid stamp. (a) A SU8 3050 master is treated with PFOCTS to facilitate later demolding. (b) Uncured PDMS mixture is poured on the master, and pressed against the hybrid stamp. (c) Due to less PFOCTS treatment on the hybrid stamp compared to the master, the casted PDMS film tends to adhere to the hybrid stamp and allows to be peeled off from the master. (d) The film is aligned and bonded by

oxygen plasma treatment (e) Remove the support PDMS on the hybrid stamp. (f) Dissolve the polystyrene plastic plate in acetone. (g) Remove the residual PDMS thin film to complete the removal of a hybrid stamp. (h) The device and top substrate are aligned and sealed without oxygen plasma bonding.

### 4.4.2. Ultra-High Precision Size-Based Particle Sorting

Figure 4-3 shows the microscope images of three different particle size mixtures (9μm+10μm), (10μm+12μm), and (10μm+15μm) at upstream focusing (Figure 4-3(a,d,g)), downstream migration (Figure 4-3(b,e,h)), and collection (Figure 4-3(c,f,i)) regions, respectively. Table 4-1 shows the size-based sorting results of the three different cases in Figure 4-3.

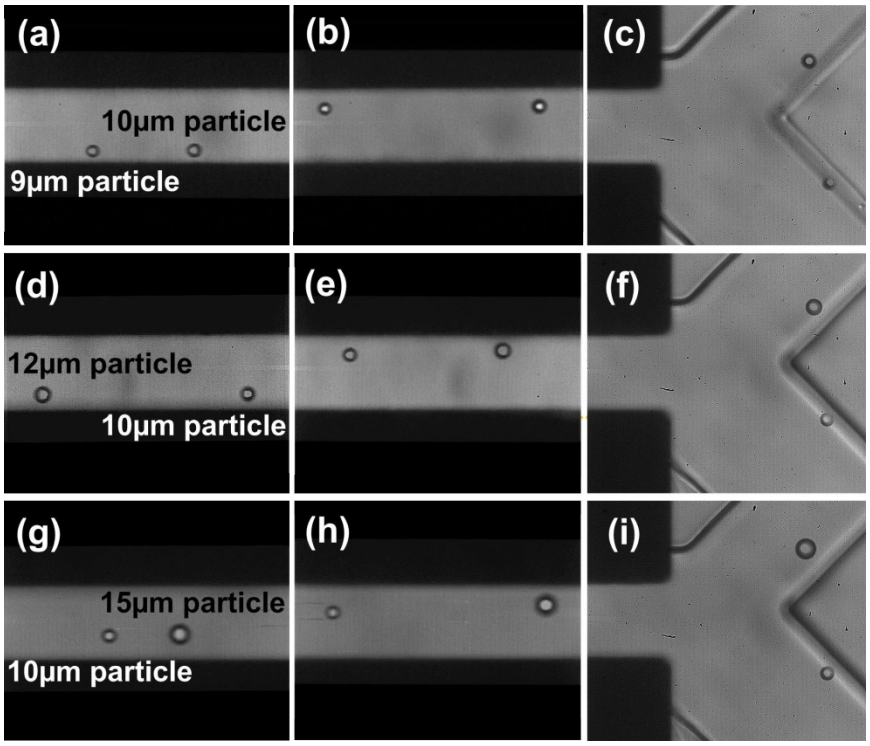

Figure 4-3 Microscopy images showing the three different particle size mixtures (9µm+10µm), (10µm+12µm), and (10µm+15µm) at upstream focusing (a,d,g), downstream migration (b,e,h), and collection (c,f,i) regions. Larger particles are collected into the upper channel.

| | **Before Sort** | **After Sort** |
|---|---|---|
| **Beads Mix** | **Purity** | **Purity** |
| 9µm+10µm | 1.2% | 94.2% |
| 10µm+12µm | 1.8% | 98.8% |
| 10µm+15µm | 1.6% | 99.1% |

Table 4-1. Size-based sorting results (purity represents the concentration of larger-sized particle).

The histograms of particle positions at locations in Figure 4-1(ii) and Figure 4-1(iii) for these three mixtures are shown in Figure 4-4. The size-independent focusing in the upstream with less than 0.2 µm standard variation of all four sizes of particles is the key to high purity sorting of particles with only 1 µm difference in size. Due to the laminar flow nature in microfluidics, the flow rate ratio between the collection (larger particles) and the waste (smaller particles) channels is around 0.5. As a result, as long as the separation of different sizes of particles

can completely fall on either side of the blue dashed lines in Figure 4-4(b, d, f), size-based particle sorting can be achieved.

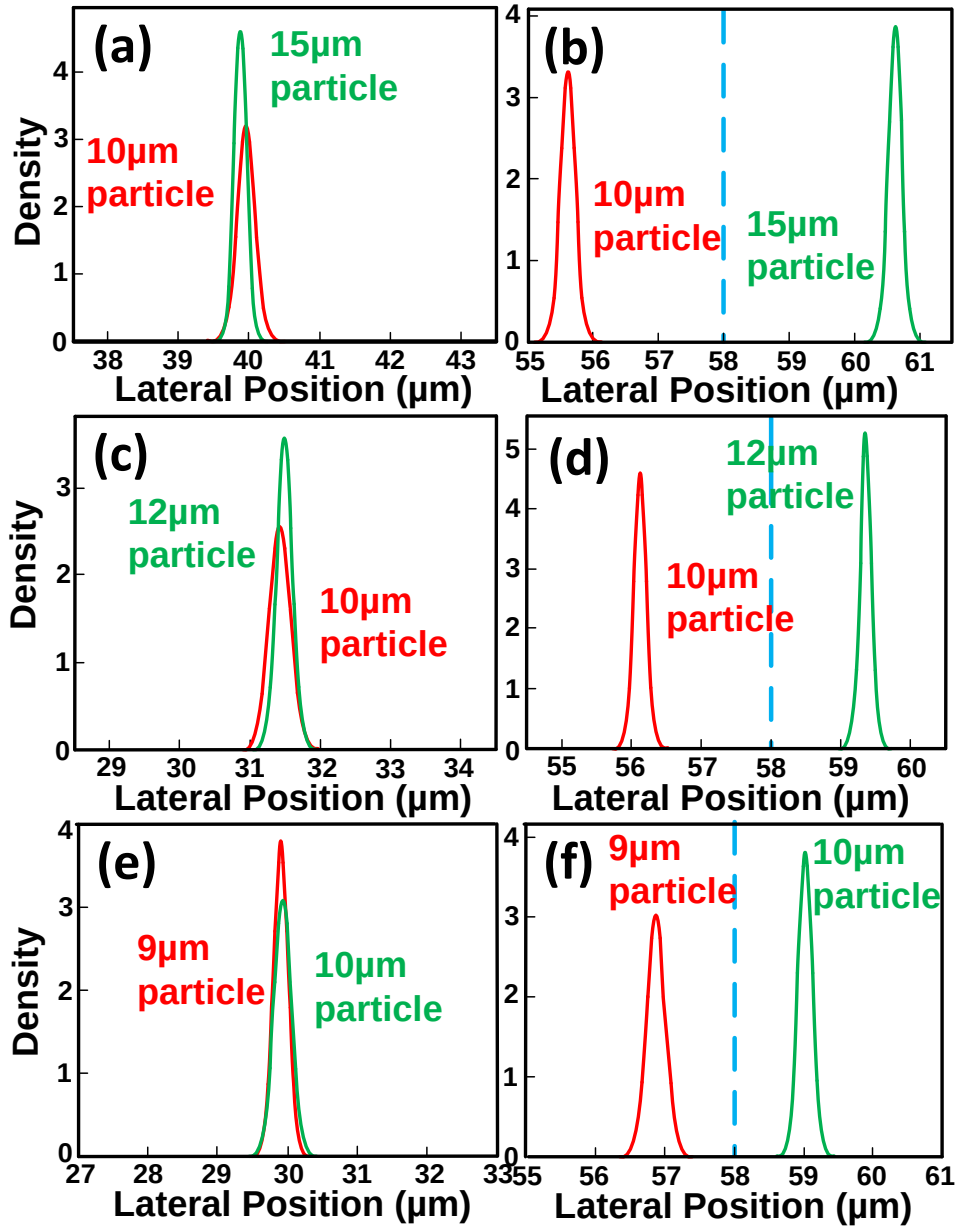


Figure 4-4: Particle position histograms at locations in Figure 4-1(ii) and Figure 4-1(iii) are shown in (a,b) for the 10µm+15µm mixture, (c,d) 10µm+12µm, and (e,f) for 9µm+10µm. Particle positions in the

upstream (a,c,e) have standard deviations of ±0.11μm, ±0.13μm, and ±0.18μm, respectively.

### 4.4.3. Rare Cancer Cell Sorting

To demonstrate the bio-compatibility of this platform, we spiked rare GFP-HeLa cells into lysed human whole blood, and did the high purity size-based sorting. The regular sizes of GFP-HeLa cells and human white blood cells fall in the range of 15μm~20μm and 8μm~12μm, respectively. The sorting results are shown in Figure 4-5. The original GFP-HeLa to white blood cell (WBC) purity is 0.4% (Figure 4-5(c)) with 94% viability (Figure 4-5(b)). After DEP sorting, the collection GFP-HeLa to WBC purity is 93.7% (Figure 4-5(d)) with 92.1% viability (Figure 4-5(b)), which corresponds to a 234 fold enrichment.

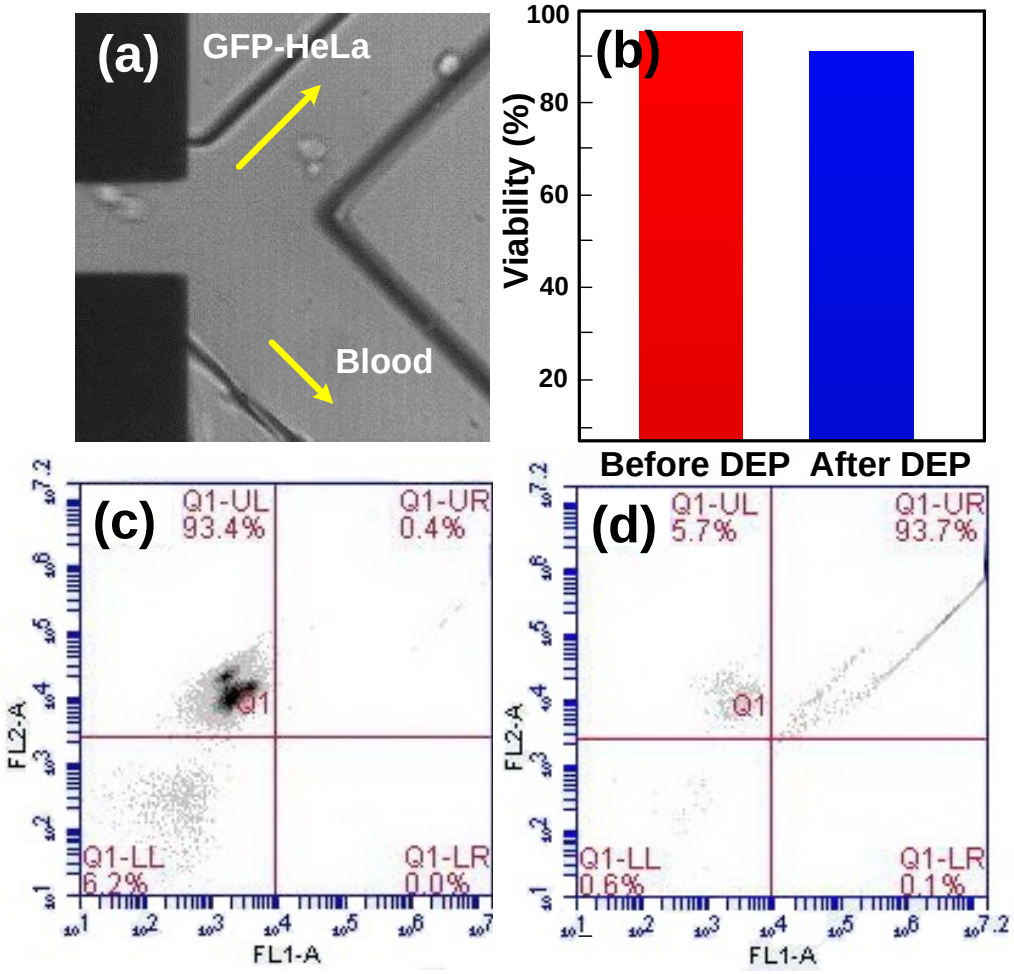


Figure 4-5: Rare cell sorting results of GFP-Hela cell spiked into lysed blood. The HeLa cell purity before and after DEP sorting purity is 0.4%(c) and 94%(d) with viability 94% and 92.1%, respectively. This corresponds to a 234 fold enrichment.

## 4.5. Reference

1. C. W. S. IV, C. D. Reyes, and G. P. López, "Microfluidic cell sorting: a review of the advances in the separation of cells from debulking to rare cell isolation," Lab on a Chip, vol. 15, pp. 1230-1249, 2015.

2. Y. Chen, T.-H. Wu, Y.-C. Kung, and P.-Y. Chiou, "3D pulsed laser triggered high speed microfluidic fluorescence activated cell sorter," in The 16th International Conference on Miniacturized Systems for Chemistry and Life Sciences, Okinawa, Japan, 2012.

3. Y. Chen, T.-H. Wu, Y.-C. Kung, M. A. Teitell, and P.-Y. Chiou, "3D pulsed laser-triggered high-speed microfluidic fluorescence-activated cell sorter," Analyst, vol. 138, pp. 7308-7315, 2013.

4. Y. Chen, T.-H. Wu, Y.-C. Kung, M. A. Teitell, and P.-Y. Chiou, "3D pulsed laser triggered high speed microfluidic fluorescence activated cell sorter," in Conference on Lasers and Electro-Optics (CLEO), San Jose, CA, U.S.A., 2013.

5. Y. J. Fan, Y.-C. Wu, Y. Chen, Y.-C. Kung, T.-H. Wu, K.-W. Huang, et al., "Three dimensional microfluidics with embedded microball lenses for parallel and high throughput multicolor fluorescence detection," Biomicrofluidics, vol. 7, p. 044121, 2013.

6. Y.-J. Fan, Y. Chen, Y.-C. Wu, Y.-C. Kung, T.-H. Wu, H.-J. Sheen, et al., "Multicolor ultra high throughput parallel microfluidic flow cytometer," in The 17th International Conference on Solid State Sensors and Actuators, Barcelona, Spain, 2013.

7. Y.-J. Fan, Y.-C. Kung, Y.-C. Wu, K.-W. Huang, T.-H. Wu, Y. Chen, et al., "High throughput fluorescence based flow cytometer using 3D microfluidics for parallel sheath flow focusing and embeded high N.A. microlens," in The 16th International Conference on Miniacturized Systems for Chemistry and Life Sciences, Okinawa, Japan, 2012.

8. H. Mohamed, L. D. McCurdy, D. H. Szarowski, S. Duva, J. N. Turner, and M. Caggana, "Development of a Rare Cell Fractionation Device: Application for Cancer Detection," IEEE Transactions on Nanobioscience, vol. 3, 2004.

9. M. Yamada, M. Nakashima, and M. Seki, "Pinched Flow Fractionation : Continuous Size Separation of Particles Ultilizing a Laminar Flow Profile in a Pinched Microchannel," Analytical Chemistry, vol. 76, pp. 5465-5471, 2004.

10. H. Amini, W. Lee, and D. D. Carlo, "Inertial microfluidic physics," Lab on a Chip, vol. 14, pp. 2739-2761, 2014.

11. F. Petersson, L. Aberg, A.-M. Swärd-Nilsson, and T. Laurell, "Free Flow Acoustophoresis: Microfluidic-Based Mode of Particle and Cell Separation," Analytical Chemistry, vol. 79, 2007.

12. U. Kim, C.-W. Shu, K. Y. Dane, P. S. Daugherty, J. Y. J. Wang, and H. T. Soh, "Selection of mammalian cells based on their cell-cycle phase

using dielectrophoresis," Proceedings of the National Academy of Sciences of the United States of America, vol. 104, pp. 20708-20712, 2007.

13. Y.-C. Kung, W. Chong, and P.-Y. Chiou, "Tunable, Sheathless, and Three Dimensional Single-Stream Cell Focusing in High Speed Flows," in The 19th International Conference on Miniacturized Systems for Chemistry and Life Sciences, Gyeongju, Korea, 2015.

14. Y.-C. Kung, K.-W. Huang, and P.-Y. Chiou, "Flow-Decoupled Dielectrophoresis for Sheathless 3D Focusing in High Speed Flows," in The 18th International Conference on Miniacturized Systems for Chemistry and Life Sciences, San Antonio, TX, U.S.A., 2014.

15. K.-W. Huang, Y.-C. Kung, Y.-C. Wu, Y.-J. Fan, and P.-Y. Chiou, "Optoelectronic Tweezers Integrated with 3D Microfluidic Networks," in 2013 International Conference on Optical MEMS and Nanophotonics, Kanazawa, Japan, 2013.

16. Y.-C. Kung, K.-W. Huang, Y.-J. Fan, and P.-Y. Chiou, "Fabrication of 3D high aspect ratio PDMS microfluidic networks with a hybrid stamp," Lab on a Chip, vol. 15, pp. 1861-1868, 2015.

17. Y.-C. Kung, K.-W. Huang, Y. Yang, Y.-J. Fan, and P.-Y. Chiou, "Fabrication of 3D microfluidic networks with A hybrid stamp," in The

26th International Conference on Micro Electro Mechanical Systems, Taipei, Taiwan (R.O.C.), 2013.

# CHAPTER 5

## CONCLUSION

We have proposed a novel fabrication methodology that enables heterogeneous integration of 3D microfluidics with hard substrates with high performance electronics. It is realized by utilizing a hybrid stamp with a thin plastic sheet embedded underneath a PDMS surface. This hybrid stamp solves an important edge protrusion issue during PDMS molding process while maintaining necessary stamp elasticity to ensure the removal of PDMS residues at through-layer regions. Removing edge protrusion is a significant progress toward fabricating 3D structures since high aspect ratio PDMS structures with flat interfaces can be realized to facilitate multilayer stacking and bonding with hard substrates. Our method also allows for the fabrication of 3D deformable channels, which can lead to profound applications in electrokinetics, optofluidics, inertial microfluidics, and other fields where the shape of channel cross-section plays a key role in device physics.

To demonstrate the potential applications, we first fabricated a microfluidic channel by sandwiching two high aspect ratio PDMS membranes between two featureless ITO glass substrates. By applying an electrical bias to the two ITO substrates and a pressure to deform

the thin membrane sidewalls, strong electric field enhancement can be generated in the center of a channel to enable 3D sheathless dielectrophoretic focusing of biological objects including mammalian cells and bacteria in high-speed flows.

We also demonstrated a novel tunnel dielectrophoresis (TDEP) mechanism for tunable, sheathless, three dimensional, and single-stream microparticle and cell focusing in high-speed flows. This new approach provides, for the first time, real-time three dimensional tuning of focusing locations by simply changing voltage combinations applied to electrodes. In addition, microparticle and mammalian cell focusing is achieved in high-speed flow in regular physiological buffers, without medium swapping to low ionic isotonic buffers as in most prior DEP based devices.

In addition, we elegantly utilized the beauty of TDEP platform on ultra-high precision microparticle and cell focusing and separation in high-speed flows. For the first time, particle size difference as small as 1μm can be separated with high purity (>90%). This is realized by a 3D tunable, size-independent, single-stream sub-micron precision (variation <0.2 μm) focusing function. Tunable electric field patterns are enabled by simply changing voltage combinations applied to electrodes.

Microparticle and mammalian cell focusing and separation is achieved at high-speed flows in high conductivity regular physiological buffers.